Molecular Therapy
Nucleic Acids
Original Article

miR-106b is a novel target to promote muscle regeneration and restore satellite stem cell function in injured Duchenne dystrophic muscle

Lara Rodriguez-Outeiriño,[1,2,10] Francisco Hernandez-Torres,[1,2,10] Felicitas Ramirez de Acuña,[1,2] Alberto Rastrojo,[3] Carlota Creus,[4] Alejandra Carvajal,[4] Luis Salmeron,[5] Marisol Montolio,[6,7] Patricia Soblechero-Martin,[8] Virginia Arechavala-Gomeza,[8,9] Diego Franco,[1,2] and Amelia Eva Aranega[1,2]

[1]Cardiac and Skeletal Myogenesis Group, Department of Experimental Biology, University of Jaen, Jaen 23071, Spain; [2]Cardiac and Skeletal Myogenesis Group, MEDINA Foundation, Center for Excellence in Research of Innovative Medicines in Andalusia, Granada 18016, Spain; [3]Department of Biology, Autonomous University of Madrid, Madrid 28049 Spain; [4]Servicio de Neurología, Hospital Universitario Virgen de las Nieves, Granada 18014, Spain; [5]Servicio de Cirugía Vascular, Hospital Universitario San Cecilio, Granada 18016, Spain; [6]Department of Cell Biology, Physiology and Immunology, Faculty of Biology, University of Barcelona, Barcelona 08028, Spain; [7]Duchenne Parent Project Spain C/ de Embajadores 128, Madrid 28045, Spain; [8]Neuromuscular Disorders Group, Biocruces Bizkaia Health Research Institute, Barakaldo, Biscay 48903, Spain; [9]Ikerbasque, Basque Foundation for Science, Bilbao 48013, Spain

Satellite cells (SCs), muscle stem cells, display functional heterogeneity, and dramatic changes linked to their regenerative capabilities are associated with muscle-wasting diseases. SC behavior is related to endogenous expression of the myogenic transcription factor MYF5 and the propensity to enter into the cell cycle. Here, we report a role for miR-106b reinforcing MYF5 inhibition and blocking cell proliferation in a subset of highly quiescent SC population. miR-106b down-regulation occurs during SC activation and is required for proper muscle repair. In addition, miR-106b is increased in dystrophic mice, and intramuscular injection of antimiR in injured mdx mice enhances muscle regeneration promoting transcriptional changes involved in skeletal muscle differentiation. miR-106b inhibition promotes the engraftment of human muscle stem cells. Furthermore, miR-106b is also high in human dystrophic muscle stem cells and its inhibition improves intrinsic proliferative defects and increases their myogenic potential. This study demonstrates that miR-106b is an important modulator of SC quiescence, and that miR-106b may be a new target to develop therapeutic strategies to promote muscle regeneration improving the regenerative capabilities of injured dystrophic muscle.

INTRODUCTION

Muscle regeneration is affected in muscle-wasting diseases like Duchenne Muscular Dystrophy (DMD),[1] a severe genetic disorder that causes progressive muscle waste in affected individuals for which there is currently no cure. DYSTROPHIN, the protein product of the gene defective in DMD, plays a pivotal structural role in anchoring muscle fiber to the extracellular matrix in the muscle niche.[2] DYSTROPHIN is also expressed in muscle satellite cells (SCs). Previous works have shown that dystrophic SCs are impaired in several SC life cycle aspects, which impact their muscle regenerative functions.[3,4] Upon activation, SCs, which are characterized by Pax7 transcription factor expression, undergo symmetric and asymmetric divisions. Asymmetrically dividing cells generate both committed progeny ($PAX7^{pos}$/$MYF5^{pos}$ cells) and offspring, whose stem cell identity remains ($PAX7^{pos}$/$MYF5^{neg}$ cells), whereas symmetric expansion helps to replenish the stem cells pool.[5] A fine balance between self-renewal and differentiation is necessary to preserve the satellite stem cell pool and to give rise to a suitable number of myogenic progenitors for proper muscle repair. Remarkably, it has been shown that dystrophic SCs display a few asymmetric divisions, which are needed to generate myoblasts and lead to a low generation rate of myogenic precursor cells.[4] Moreover, dystrophic muscle fibers cultured for 72 h display an increase in the subset of $PAX7^{pos}$ SCs that never express myogenic factor MYF5, with a reduction in the number of MYOG-expressing progenitors,[6] which further suggests that dystrophic SCs can also display enhanced self-renewal. Hence, research to restore the SC function has attracted much interest in recent years, and the intention is to develop new strategies to treat muscle regeneration intrinsic defects in DMD.

In the context of SC biology, microRNAs (miRNAs) play a critical role in regulating muscle regeneration and SC behavior. Therefore, lack of miRNA-processing endoribonuclease DICER1 leads to the depletion of SCs and the quasi-absence of repair upon injury.[7] miRNAs, like miR-195 and miR-497, are particularly involved in SC cell-cycle arrest during the juvenile to adult phase transition,[8] and miR-489 targets oncogene Dek to prevent cell cycle re-entry.[7]

Received 18 February 2022; accepted 14 August 2022;
https://doi.org/10.1016/j.omtn.2022.08.025.

[10]These authors contributed equally

Correspondence: Amelia Eva Aranega, PhD, Cardiac and Skeletal Myogenesis Group, Department of Experimental Biology, University of Jaen, Jaen 23071, Spain.
E-mail: aaranega@ujaen.es

miR-31 also binds to *Myf5* mRNA and is, thus, sequestered in messenger ribonucleoprotein (mRNP) granules, which represses its translation until SCs re-enter the cell cycle.[9] Recently, a *Notch*-miR-708-*Tns3* axis has been described to modulate SC quiescence and transition to the activation state through the dynamic regulation of migratory machinery.[10] These findings generally indicate the potential of miRNAs as powerful molecular tools to regulate the satellite function in the muscle regeneration and disease context.

As we previously identified miR-106b as a member of a Pitx2-miRNA pathway, which regulates the cell proliferation and myogenic commitment of SCs,[11,12] we hypothesize that miR-106b may play a role in SC myogenic progression during muscle regeneration and could have an impact by modifying SC behavior in the muscle dystrophies context.

RESULTS

miR-106b reinforces quiescence in Myf5^{neg} SCs and its expression is down-regulated after muscle injury

We previously identified miR-106b as a member of a *Pitx2*-miRNA pathway that regulates the cell proliferation and myogenic commitment of early activated SCs by targeting cell-cycle regulatory genes *Ccnd1* and *Ccnd2*, and also myogenic factor *Myf5*.[11] This led us to wonder whether miR-106b plays a role in SC myogenic progression in the muscle injury and regeneration context. First, we further analyzed the expression pattern of miR-106b in mouse adult muscle. miR-106b expression was only detected in a proportion (~13%) of PAX7^{pos} SCs, we also observed that miR-106b^{pos} cells were MYF5^{neg} (Figure 1A). Next, we performed *in vitro* experiments of gain- and loss-of-function in freshly isolated SCs by using lentiviral particles bearing the miR-106b mimic (premiR), miR-106b inhibitory (antimiR) and Scramble-control molecules. After 3 days of premiR lentiviral transduction, only the non-transduced myogenic MYOD1^{pos} proliferating (KI67^{pos}) cells were observed (Figure 1B), as miR-106b overexpression led to inactive free-floating SCs after lentiviral transduction that remain floating after 5 days in culture while antimiR-transducted SCs display enhanced differentiation (Figure S1A). This cell phenotype might be a consequence of miR-106b effects that target cell-cycle regulatory genes, as we previously reported.[11] Consistently with this, antimiR-transduction clearly increased the pools of proliferating activated MYOD1^{pos}/KI67^{pos} cells in culture (Figure 1B). In addition, lentiviral antimiR-transduction in freshly isolated SCs led to Myf5 up-regulation, which was accompanied by the down-regulation of quiescence marker Cd34 mRNA,[13,14] whereas premiR transduction induced low Myf5 mRNA levels, but high Cd34 mRNA levels (Figure S1B). This scenario suggests that miR-106b maintains SCs in a high quiescent state. If miR-106b can promote the quiescence of SCs, its down-regulation would be related to SC activation. According to this idea, we found that miR-106b was present in the PAX7^{pos} quiescent SCs of freshly isolated myofibers, but we did not detect any miR-106b expression in the activated SCs (MYOD1^{pos}) after 48 h of myofiber cultures (Figure 1C). We also checked the impact of miR-106b inhibition on asymmetric division in the isolated SCs following a previously described cell-cycle synchronization strategy combined with Pax7 and MyoD1 labeling to examine the fate of newly divided daughter cells.[15] We found that doublets of sister cells in the antimiR-106b transduced cells were predominantly PAX7^{pos}MYOD1^{pos}:PAX7^{pos}MYOD1^{neg} and PAX7^{pos}MYOD1^{pos}:PAX7^{neg}MYOD1^{pos}, which represent asymmetric self-renewal and asymmetric differentiation divisions and, as a consequence of an increase in cell division, the total number of MYOD1^{pos} was higher in the antimiR-transduced cells (Figure 1D). All these findings suggest that miR-106b expression confers a strong quiescent stemness status, while its down-regulation leads to SC activation and proliferation with predominant asymmetric cell division.

In addition, the relevance of miR-106b reinforcing quiescence in an SC population subset was highlighted by two facts; first, miR-106b was the main miRNA of its miR-family (miR17-family) to be expressed in freshly isolated quiescent SCs (Figures S2A and S2B); second, the high capability to modify Myf5 mRNA stability versus other miRNAs, which also targeted this transcription factor, such as miR-31 (Figure S2C).[9]

Next, we analyzed miR-106b behavior during muscle regeneration in mice. Our results clearly showed that miR-106b was down-regulated within the time window that comprised days 3 and 7 after cardiotoxin (CTX) injection in the tibialis anterior (TA) muscle of the C57BL/6 mice (Figure 2A). Interestingly, a strong and statistically significant up-regulation of myogenic factors Myf5, Myod1, and Myog in regenerating muscle was observed on day 3 after CTX injection (Figure 2A). This finding supports the notion that miR-106b down-regulation is associated with myogenic differentiation during muscle regeneration.

miR-106b inhibition induces myogenesis differentiation and enhances muscle regeneration

In order to further characterize the role of miR-106b during muscle repair, we followed an *in vivo* miR-106b gain- and loss-of-function approach by injecting CTX together with premiR or antimiR-106b molecules in TA muscles (Figures 2B and S2D). Notably, miR-106b manipulation in TA did not bring about any significant compensatory changes in the levels of other miR-17 family members (Figures S2E and S2F). Three days after intramuscular injection, the number of proliferating MYOD1^{pos}/KI67^{pos} cells significantly lowered in the CTX- and premiR-injected muscles. On the contrary, the number of proliferating committed MYOD1^{pos}/KI67^{pos} cells significantly increased in the antimiR-treated muscles (Figure 2C). As a result, muscle regeneration was enhanced, as observed by the largest number of differentiating eMyHC^{pos} new myofibers on day 7 of antimiR and CTX injection (Figure 2D). The morphometric measurements revealed a narrower size variation for the regenerating eMyHC^{pos} myofibers, which became smaller in the TA treated with antimiR than in the control muscles (Scramble-treated) on day 7 of injury (Figure 2D). However, the fiber measurements taken on day 15 after muscle damage in the antimiR-treated muscles revealed an increase of the larger myofiber sizes (Figure 2E) and a higher fusion index (Figure 2F), which suggest more mature fiber formation. Nonetheless, premiR-injected muscles displayed an increase in the number of

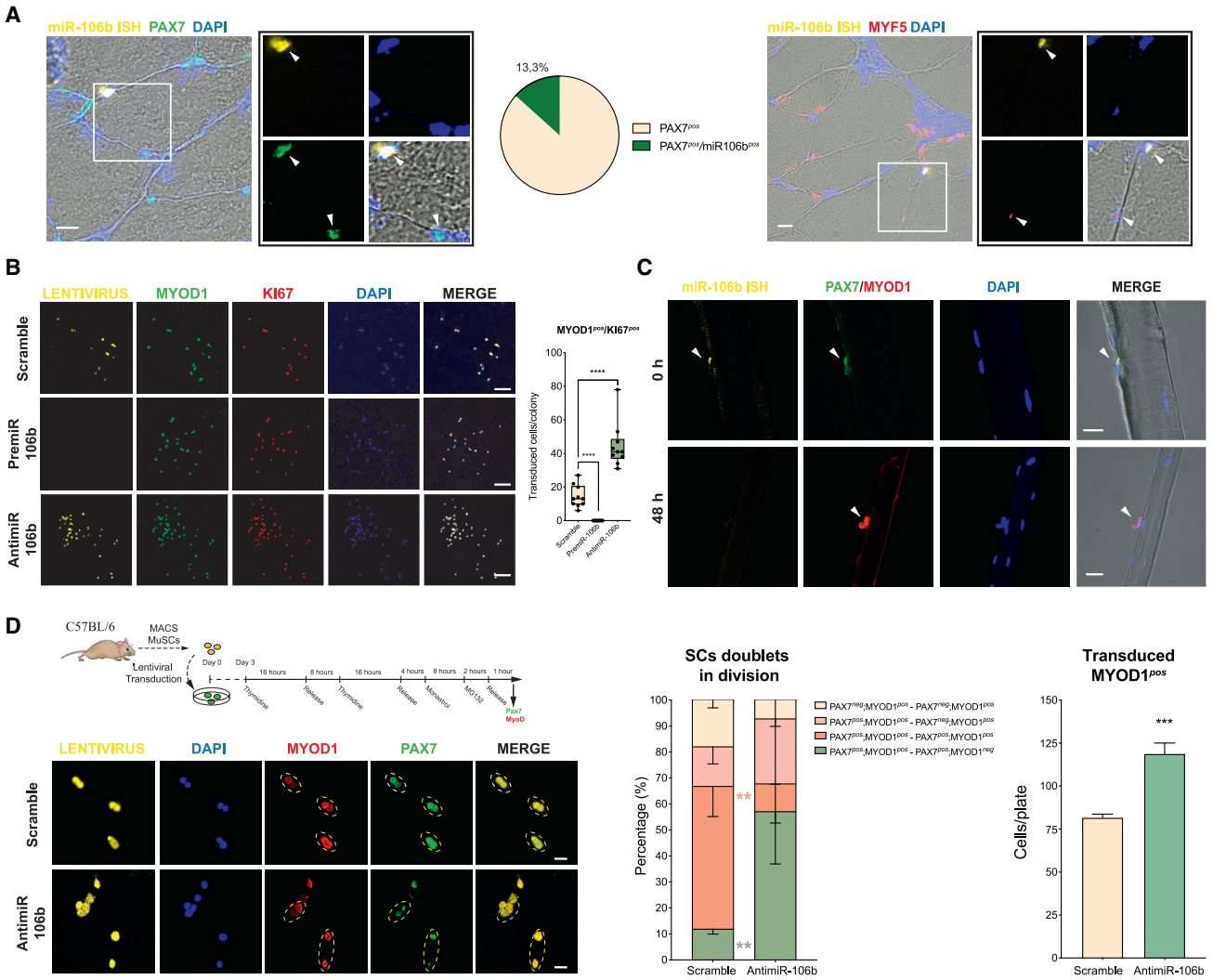

Figure 1. miR-106b is expressed in PAX7^{pos}/MYF5^{neg} SCs, represses proliferation and differentiation, and its inhibition leads to the cell activation state

(A) total of 18 C57BL/6 male mice, aged 4–6 months, were randomized into three groups: LNA *in situ* hybridization for miR-106b, miR-106b gain, and miR-106b loss-of-function experiments *in vitro,* cultured single myofibers at 0 and 48 h and synchronizing cultures in the late telophase stage (n = 3 per condition and time point). A fluorescence *in situ* hybridization for miR-106b and the immunofluorescence staining of PAX7 and MYF5 in the TA section from C57BL/6 mice. Quantification of the miR-106b^{pos}/PAX7^{pos} cells is shown (six sections per mouse; five fields per section). (B) The MYOD1 and KI67 staining of the cultured SCs from C57BL/6 mice hindlimb muscles 72 h after premiR, antimiR or control Scramble lentiviral transduction. Quantification of MYOD1^{pos}/KI67^{pos} cells per colony (n = 3 independent experiments; 20 cell colonies). (C) Fluorescence *in situ* hybridization for miR-106b and the immunofluorescence staining of PAX7 and MYOD1 in single EDL myofibers from the C57BL/6 mice cultured for 0 and 48 h (three mice; n = 15 fibers). (D) Strategy for synchronizing the cultured SCs in the late telophase stage after lentiviral transduction (yellow), and representative images of the lentiviral-transduced SCs synchronized in the telophase stage and stained for PAX7 (green) and MYOD1 (red). Percentages of the asymmetric self-renewal (PAX7^{pos}/MYOD1^{pos}:PAX7^{pos}/MYOD1^{neg}), symmetric proliferative (PAX7^{pos}/MYOD1^{pos}:PAX7^{pos}/MYOD1^{pos}), asymmetric differentiation (PAX7^{pos}/MYOD1^{pos}:PAX7^{neg}/MYOD1^{pos}), and symmetric differentiation (PAX7^{neg}/MYOD1^{pos}:PAX7^{neg}/MYOD1^{pos}) divisions are shown (n = 3 independent experiments, 15 doublets per condition). Quantification of the total number of transduced MYOD1^{pos}:cells is shown. Scale bars, 20 μm (A, C, and D), 100 μm (B). Data are presented as mean ± SD. **p < 0.01; ***p < 0.001; p < 0.0001.

very small regenerating myofibers on 7 and 15 days of injury (Figures 2D and 2E). A lesser increase in fusion index was also observed in premiR-treated muscles with respect to control scramble-injected (Figure 2F), this fact might be due to premature myoblast fusion after accelerated exit of cell cycle induced by pre-miR-treatment. These results indicate that miR-106b inhibition facilitates muscle regeneration, while large doses of miR-106b lead to an abnormal muscle repair pattern, which indicates that miR-106b decay is required for proper muscle repair.

It was noteworthy that antimiR-106b treatment did not affect the re-entry of SCs into quiescence after muscle repair, as revealed by a non-statistically significant trend of a larger total number of PAX7^{pos} sublaminar cells in the antimiR-treated muscles 30 days after

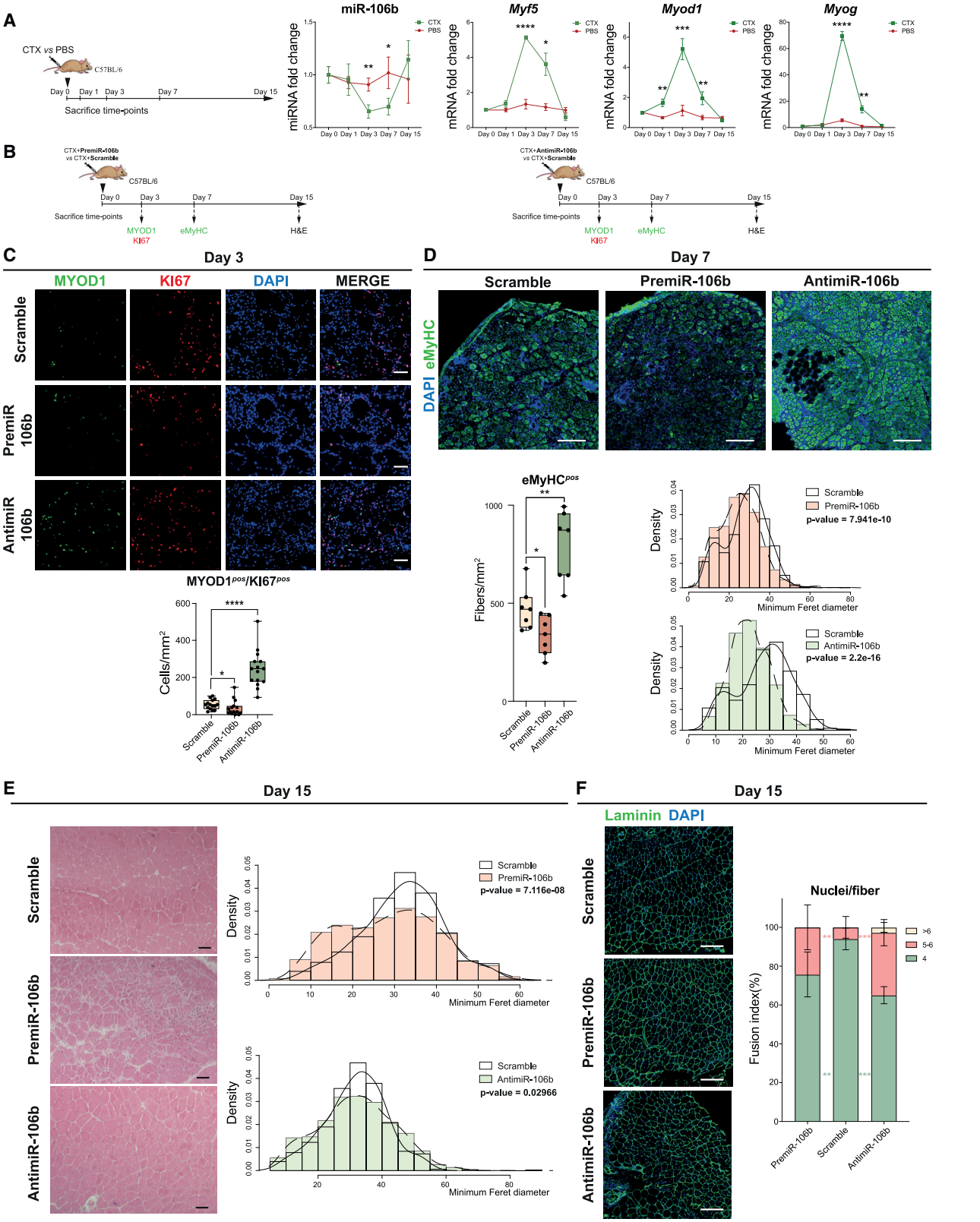

(legend on next page)

injury (Figures 3A and 3B), with no changes noted in the number of MYOD1^{pos} sublaminar cells (Figures 3A–3C), as previously described as committed SCs.[16] Furthermore, the SCs in the TA treated with a single antimiR injection continued to robustly contribute to muscle repair after re-injury, as noted by an increase in both the fiber diameter and the number of centralized nuclei at day 7 after re-injury in the previously antimiR-injected muscles (Figure 3D). Similar to that found after first muscle injury, a non-significantly larger number of PAX7^{pos} sublaminar cells in the re-injured antimiR-treated muscles was observed (Figure 3E). Collectively, all these findings indicate the relevance of miR-106b inhibition as a potential valuable approach to induce muscle regeneration.

miR-106b is highly expressed in mouse dystrophic SCs and *in vivo* antimiR-106b treatment enhances the skeletal muscle regenerative potential in dystrophic mice

Next, we looked for the miR-106b expression in a context in which muscle regeneration is not successfully completed by using the dystrophic-deficient mdx mouse model of DMD.[17] miR-106b was expressed in mdx mouse muscles (Figure 4A) in a similar proportion to that found in wild-type mice (data not shown). We also found that miR-106b had increased in the muscles and isolated SCs of the dystrophin-deficient mdx mice (Figures 4B and 4C) and, contrary to that observed for the wild-type SCs, high miR-106b expression levels were maintained on culture day 5 (Figure 4C), which is consistent with the maintenance of the quiescence and a previously reported reduced proliferating capacity for dystrophic SC populations.[4,12,18] Furthermore, miR-106b loss-of-function clearly increased the number of MYOG^{pos} myoblasts (Figure 4D), which indicates that antimiR treatment enhances the onset of myogenic differentiation of dystrophic SCs.

In order to address whether miR-106b inhibition could modulate muscle regeneration in mdx mice, the TAs of the 4-month-old mdx mice were injected with CTX and antimiR-106b. The lower miR-106b levels induced by antimiR injection were concomitant with the up-regulation of Myf5, MyoD1, and Myog, which suggests that miR-106b inhibition could induce myogenic differentiation (Figure 5A). We further checked for cells in the G-Alert state, in which SCs were "primed" to rapidly respond under stress or injury conditions.[19] We observed that the *in vivo* antimiR injection enhanced the number of SCs positive for G-Alert-marker PS6 (Figure S3), and also increased the number of proliferating MYOD1^{pos}/KI67^{pos} 3 days after antimiR injection (Figure 5B). These findings suggest that antimiR-106b treatment enhances the functional ability of dystrophic SCs to activate and participate in tissue repair.

The immunohistochemical and histological analyses revealed that the number of eMyHC^{pos} myofibers and the amount of regenerating larger myofiber sizes were enhanced in the dystrophic TA muscles on day 7 after antimiR injection (Figure 5C). In addition, an increase in the percentage of fibers with centralized nuclei and an enlargement in the larger myofibers sizes on day 15 in antimiR-treated compared with control scramble-injected muscles were observed (Figure 5D), as well as a highest fusion index (Figure 5E). These findings indicate that the regenerative potential was enhanced in the mdx-SCs after antimiR injection. Functional performance was assayed by treadmill tests in the mdx mice injected with CTX + antimiR-106b until exhaustion 30 days after antimir treatment. As illustrated in Figure 5F, both the running time and distance were respectively 50% and 95% longer in the antimiR-treated mice compared with the control, which indicates that the antimiR injection boosts physical performance.

To further elucidate the effects of antimiR-106b injection during muscle regeneration in a context in which miR-106b is deregulated, such as the dystrophic muscle, we examined the transcriptome profile changes mediated by antimiR treatment at day 3 and day 7 after CTX injection in mdx mice by the RNA-sequencing (RNA-seq) analysis (Figure 6). This analysis revealed that the number of differentially expressed genes between days 3 and 7 after CTX injection was higher (6,278) in antimiR-treated muscles than in the control Scramble-injected mice (3,244) (Figures 6A and 6B). AntimiR-106b and scramble-treated dystrophic muscles shared 2,985 differentially genes between day 3 and day 7 after CTX injection (Figures 6A and 6B). Note that 3,293 genes were only deregulated in antimiR-106b-treated muscles and 259 genes were only deregulated in scramble-treated muscles. Moreover, since the number of differentially expressed genes between antimiR-treated and scramble-injected muscles were clearly higher at day 3 (426) than at day 7 (9) (Figures 6A and 6B), we concluded that the changes in the transcriptome profile induced by antimir treatment occurred mainly on day 3. This is consistent with the transient down-regulation of miR-106b after antimir treatment is mostly observed at day 3.

Interestingly, the GO-biological process and cellular component ORA-analysis in the antimiR-treated dystrophic muscles after injury

Figure 2. miR-106b is down-regulated after muscle injury and its inhibition enhances muscle regeneration

(A) Scheme of CTX injection in the C57BL/6 male mice TA, and the transcript levels of miR-106b, *Myf5*, *MyoD1,* and *Myog* in TA muscle. CTX was injected in TA and PBS injected into contralateral muscle and used as a control. n = 15 mice randomized into five groups: days 0, 1, 3, 7, and 15 after injection) (n = 3 per time point). (B) Scheme of the CTX + premiR-106b or antimiR-106b injection in the C57BL/6 mice TA. CTX + scramble was injected into contralateral muscle and used as a control. n = 18 mice randomized into three groups: days 3, 7, and 15 after intramuscular injections (n = 3 per group). (C) MYOD1 and KI67 immunostaining on the TA section from scramble and premiR or antimiR (3 days post-administration). Quantification of the percentage of the MYOD1^{pos}/KI67^{pos} cells is shown. (D) eMyHC staining on the TA section from scramble and premiR or antimiR (7 days post-administration) and quantification of the number per area and minimum Feret's diameter distribution (μm) of the eMyHC^{pos} myofibers. (E) H&E staining on the TA section from scramble and premiR or antimiR (15 days post-administration) and muscle fiber size distribution analyzed by Minimal Feret Diameter (μm) is shown. (F) Immunofluorescence for Laminin on the TA section from scramble and premiR or antimiR (15 days post-administration) and the fusion index is shown. Scale bars, 50 μm (C), 200 μm (D–E). Data are presented as mean ± SD.*p < 0.05; **p < 0.01; ***p < 0.001; ****p < 0.0001.

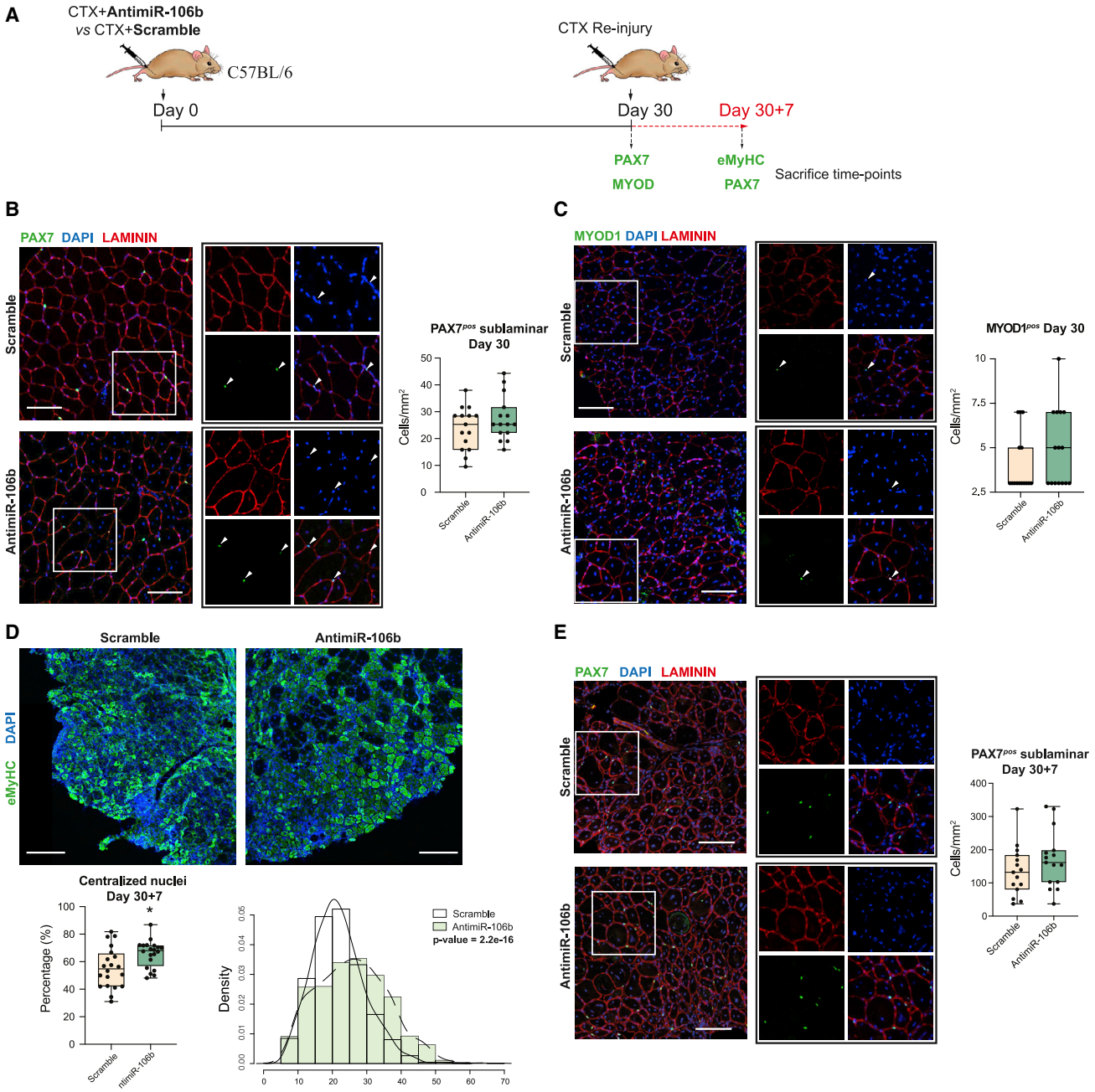

Figure 3. Single antimiR-106b injection continues to contribute to muscle repair after re-injury

(A) Scheme of CTX+ antimiR versus Scramble injection and re-injury in the C57BL/6 male mice TA. Six mice were randomized into two groups CTX + scramble versus CTX + antimiR injected at 30 days post-injection and CTX + scramble versus CTX + antimiR injected at 30 days post-injection + 7 days after re-injury (n = 3 per group). (B) Representative images of LAMININ and PAX7 staining on the TA sections from the scramble and antimiR-injected TA muscles (30 days post-administration). Quantifications of the number of PAX7^{pos} is shown. Scale bars, 40 μm. (C) Representative images of LAMININ and MYOD1 staining on the TA sections from the scramble and antimiR-injected TA muscles (30 days post-administration). Quantifications of the number of MYOD1^{pos} sublaminar cells are shown. Scale bars, 40 μm. (D) Immunofluorescence staining of eMyHC in the TA sections from scramble and antimiR (30 days post-administration + 7 days after re-injury). The percentage of centralized nuclei and muscle fiber size distribution (analyzed by Minimal Feret Diameter [μm]) in eMyHC^{pos} myofibers are shown. (E) Representative image of the PAX7^{pos} sublaminar cells in the antimiR-106b-treated re-injured muscles; quantification of the number of PAX7^{pos} sublaminar cells is shown. Scale bars, 200 μm. Data are presented as mean ± SD. *p < 0.05.

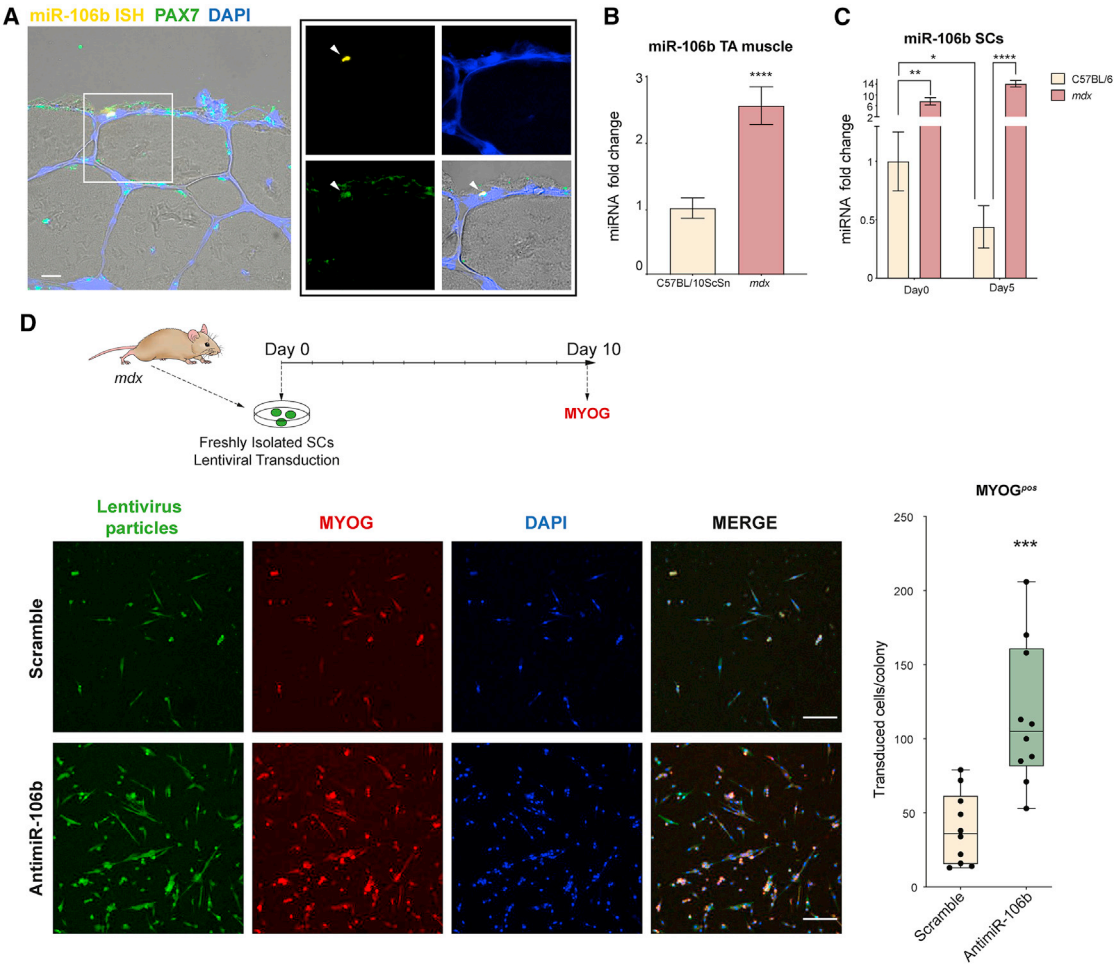

Figure 4. miR-106b is enriched in mdx-SCs and modulates their differentiation capabilities

A total of 15 male mdx and three C57BL/6 male mice, aged 4–6 months, were randomized into four groups: the LNA *in situ* hybridization analyses, RT-qPCR analyses in TA muscles, RT-qPCR analyses in cell cultures, miR-106b loss-of-function experiments *in vitro* (n = 3 per group). (A) Fluorescence *in situ* hybridization for miR-106b and the immunofluorescence staining of PAX7 on a TA section from the mdx mice. (B) Transcript levels of miR-106b in the TA from mdx mice hindlimb muscles. (C) Transcript levels of miR-106b in freshly isolated quiescent SCs from C57BL/6 and mdx mice on day 0 versus the 5-day cultured SCs (1,500–2,000 cells). (D) Scheme of antimiR lentiviral transduction in freshly isolated mdx-SCs and MYOG staining; quantification of the number of lentiviral-transduced $MYOG^{pos}$ nuclei per cell colony 10 days after treatment (10 colonies per mouse). Scale bars, 20 μm (A), 100 μm (D). Data are presented as mean ± SD. *p < 0.05; **p < 0.01; ***p < 0.001; ****p < 0.0001.

revealed an enrichment in gene sets related to skeletal muscle differentiation, such as myofibril, striated muscle cell differentiation, actin filament organization, or actin filament-based (Figures 6C–6E). Nonetheless, in control Scramble-injected dystrophic muscle gene sets linked to inflammatory process, such as acute inflammatory response or regulation of production of molecular mediator of immune response, were enriched (Figures 6D and 6E). Those findings reinforce the notion that antimiR treatment increases muscle regeneration in dystrophic mice after injury, but also indicate that the persistent inflammation associated to the dystrophic muscle might be attenuated,[20] a finding probably linked to enhanced muscle regeneration.

Finally, the impact of antimiR-106b treatment on dystrophic muscles was further validated by the DBA/mdx mouse model, a DMD model that better recapitulates several human characteristics of DMD myopathology (https://www.jax.org/jax-mice-and-services). AntimiR-106b injection in the TA muscle of DBA2J/mdx mice also boosted the differentiation kinetics of SCs, as observed by an increased number of $KI67^{pos}$/$MYOD1^{pos}$ cells on day 3 after induced muscle damage (Figures 7A and 7B). Because DBA/mdx mice exhibit a retarded and impaired muscle regeneration,[21–23] $eMyHC^{pos}$ myofibers were analyzed on day 15 post-administration; we found that both the number of $eMyHC^{pos}$ myofibers and the regenerating larger myofibers sizes were increased (Figure 7C). Overall, these results reinforce the notion that antimiR-106b injection enhances muscle regeneration in the dystrophic muscle by increasing the number of myogenic progenitors after SC activation.

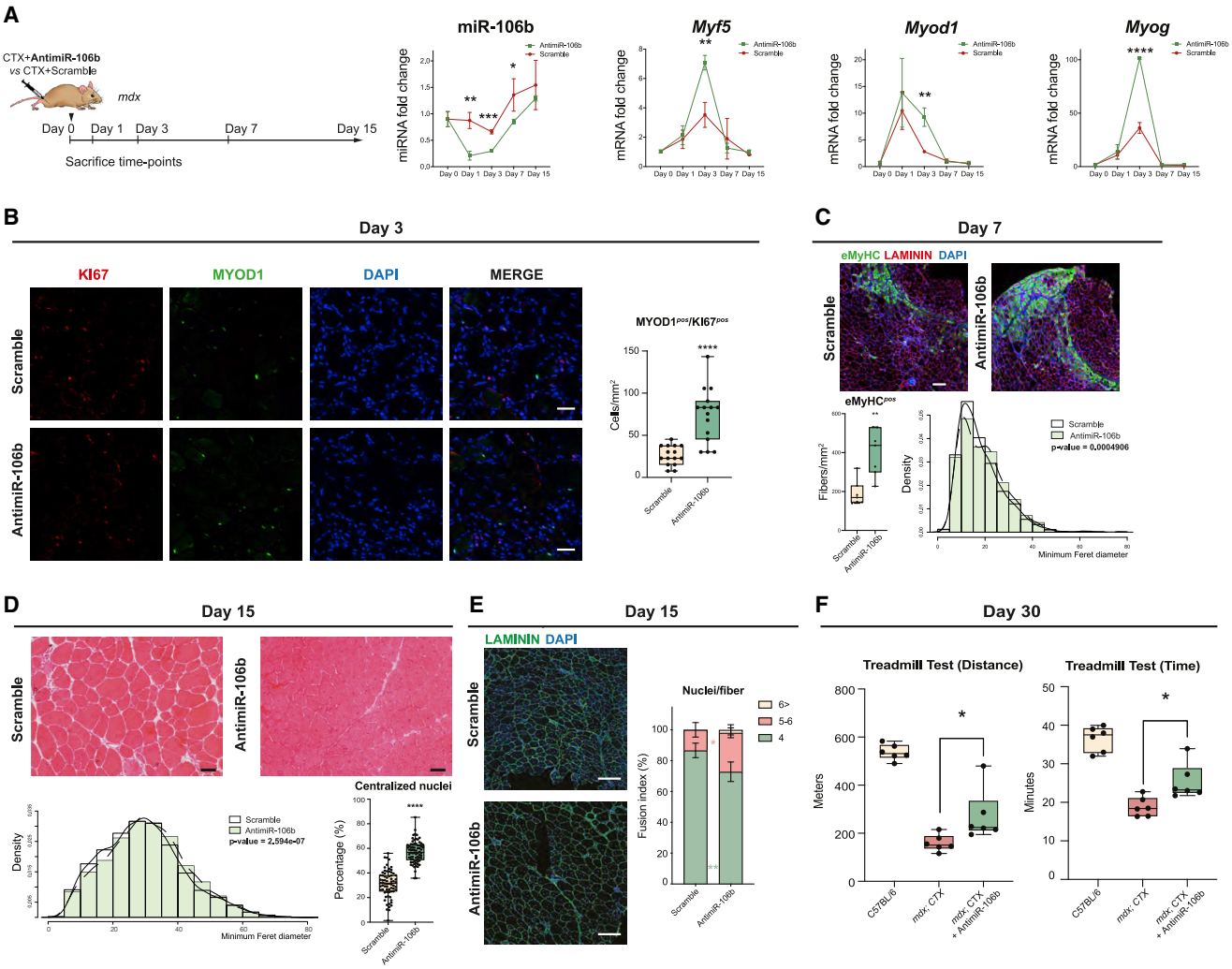

Figure 5. miR-106b inhibition enhances muscle regeneration in dystrophic mdx mice

n = 36 mdx mice, aged 4–5 months, were randomized into three groups: CTX-scramble/antimiR-injected for the RT-PCR analyses (days 0, 1, 3, 7, and 15 after injection, n = 3 per time point and condition); CTX-scramble/antimiR-injected for the immuno- and histochemical experiments (days 3, 7, and 15 after injection, n = 3 per time point and condition); CTX-Scramble and CTX-antimiR injection for the Treadmill test (n = 6 per condition). A separate batch of 6 C57BL/6 male mice, aged 4–6 months, was used for the Treadmill test. (A) Scheme of the CTX + antimiR injection in the mdx male mice TA and the transcript levels of miR-106b, *Myf5*, *MyoD1,* and *Myog* in the injured TA muscles. The control scramble + CTX were injected into the contralateral TA and used as a control. (B) MYOD1 and KI67 immunostaining on the TA section from the scramble- and antimiR-treated mdx mice (3 days post-administration). Quantification of the percentage of KI67^{pos}/MYOD1^{pos} cells are shown. (C) Immunostaining for eMyHC^{pos} myofibers in the TA section of the antimiR-treated mdx mice (7 days post-administration). The number of eMyHC^{pos} myofibers and muscle fiber size distribution (analyzed by Minimal Feret Diameter [μm]) are shown. (D) H&E staining on the mdx-TA section from scramble and antimiR (15 days post-administration). Muscle fiber size distribution (analyzed by Minimal Feret Diameter [μm]) is shown. (E) Immunofluorescence of LAMININ on the mdx-TA section from scramble and antimiR (15 days post-administration). Fusion index is shown. (F) The treadmill test in the CTX + scramble- and CTX + antimiR-treated mdx and C57BL/6 mice (30 days post-administration). Scale bars, 50 μm (B), 200 μm (C and D). Data are presented as mean ± SD. *p < 0.05; **p < 0.01; ***p < 0.001; ****p < 0.0001.

miR-106b inhibition increases the *in vitro* myogenic differentiation of human muscle stem cells and enhances its contribution to muscle regeneration after intramuscular transplantation

We next tested if miR-106b could also act in human muscle stem cells (hMuSCs). *In situ* hybridization experiments in the sections of hMuSCs revealed that miR-106b was also present in a subset of PAX7^{pos} hMuSCs (Figure 8A) at a similar ratio to that observed in mice (data not shown). The miR-106b effects on *in vitro* differentiation were evaluated by loss-of-function experiments by lentiviral transduction in freshly isolated hMuSCs from muscle biopsies. We observed that myotube formation was enhanced in the antimiR-transduced cells given a significant increase in the fusion index, which suggests that antimiR treatment also

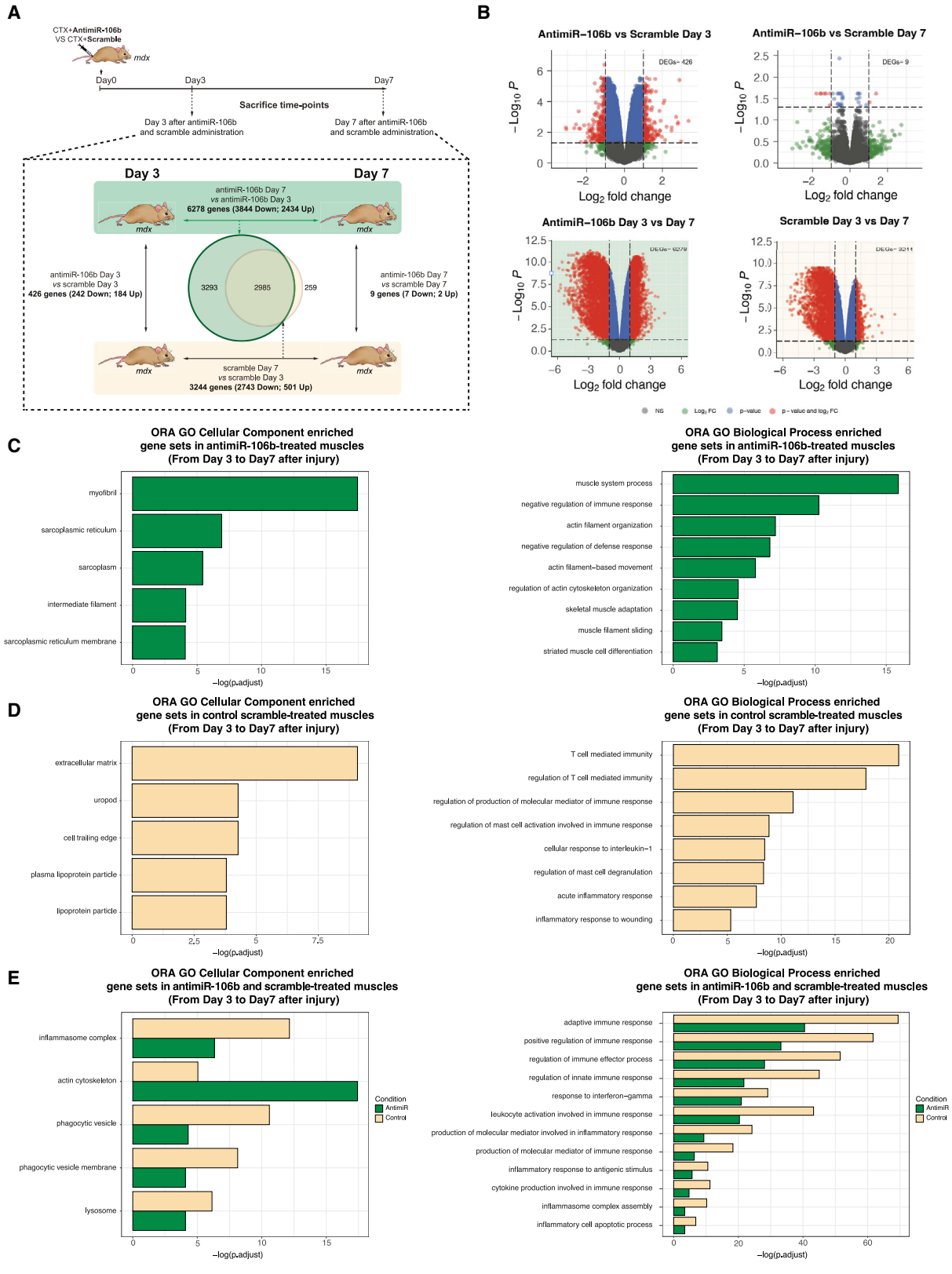

(legend on next page)

modifies the *in vitro* cell differentiation potential of hMuSCs (Figure 8B).

In order to check if miR-106b inhibition modulated the regenerative abilities of hMuSCs, we performed xenotransplantation of the hMuSCs transfected with antimiR into the pre-injured TA of immunodeficient mice. Our results showed a larger number of human-DYSTROPHIN^{pos} myofibers for antimiR-transduced cells after 5 weeks of xenotransplantation (Figure 8C). These results indicate that miR-106b inhibition promotes the engraftment and formation of human-derived myofibers.

miR-106b is high in human dystrophic muscles and modulates the myogenic potential of human dystrophic muscle stem cells

In order to investigate the role of miR-106b in the human muscular dystrophies context, we used the muscle biopsies obtained from patients with Becker Muscular Dystrophy (BMD) and DMD after obtaining written informed consent from all of them or from their legal representatives. Due to ethical issues linked with patients' age and/or the highly invasive nature of muscle biopsies, only a few patients were included in this analysis. The RT-qPCR analysis revealed higher miR-106b expression levels in the muscles of two BMD patients compared with the control muscle biopsies (Figure 9A). The hMuSCs isolated from the muscle biopsies of the BMD patients, and transduced with antimiR, significantly increased the number of myoblasts after 14 days of *in vitro* culture (Figure 9B). However, consistently with the loss of proliferative capacity of the miR-106b-overexpressing cells, no premiR-transduced cell was observed at 14 culture days.

We also noticed that the hMuSCs freshly isolated from the muscle biopsy of one DMD patient displayed higher miR-106b expression levels (Figure 9C), and they generated a smaller amount of proliferating (MYOD1^{pos}/KI67^{pos}) cells after 2 days of *in vitro* culture compared with the control hMuSCs, which gave fewer MF20^{pos} myofibers after 6 culture days in differentiation medium (Figure S4A). Interestingly, antimiR-lentiviral transduction in undifferentiated freshly isolated hMuSCs (Figure 9D) increased the number of MYOD1^{pos}/KI67^{pos} cells (Figure 9E), which led to both a larger amount and a longer length of the formed myotubes after 6 days in differentiation medium (Figure 9E). However, in immortalized human DMD-MuSC-derived myoblasts, treatment with pre-miR inhibited proliferation, further promoting differentiation, whereas the antimiR treatment maintained cell proliferation, thus impeding further differentiation (Figure S4B). This indicates that miR-106b has no effect on differentiation of dystrophic hMuSC-derived myoblasts in which the myogenic program has already been initiated. This scenario suggests that miR-106b inhibition enhanced the regenerative potential of undifferentiated dystrophic hMuSCs by increasing their capability to proliferate and to form myogenic precursors.

DISCUSSION

The understanding of muscle satellite stem cells' quiescence and activation is integral to regenerative medicine. Accumulating evidence reveals that SC behavior is widely heterogeneous in both its transition to a proliferative state and its decision to self-renew or differentiate.[6,19,24] In line with this, several previous studies support a relation between MYF5 heterogeneous expression and SC functionality. Hence the SCs that never expressed MYF5 (MYF5^{neg}) were found to give rise to a MYF5^{neg} satellite stem cell and MYF5^{pos} committed SCs, whereas the transplanted MYF5^{pos} acted as myoblasts by failing to engraft, exhibited poor survival, and fused with one another to form new myofibers.[6] Myf5 heterozygous SCs are more prone to a stem-like phenotype without it affecting their ability to generate new myofibers. However, Myf5-null SCs display a better self-renewal capacity than wild-type stem cells, but their ability to regenerate muscle is limited.[24] Despite the functional importance of these different SC subpopulations, the molecular mechanisms underlying the differences between them, and the existence of a practical marker, are still missing. Here we report the first example of an miRNA that defined a robust quiescent state in MYF5^{neg} cells. miR-106b was present in quiescent MYF5^{neg} SCs, but was down-regulated during SC activation. Moreover, miR-106b overexpression maintained SCs in a more stem-like dormant phenotype, but miR-106b inhibition facilitated asymmetric divisions by allowing them to increase the number of proliferative myogenic-committed cells. These results, together with the fact that miR-106b was down-regulated concomitantly with the first wave of myogenic differentiation during muscle regeneration, enable us to conclude that miR-106b inhibition is required for full and proper SC activation.

The normally quiescent state of SCs has also been shown to be regulated by miR-489, miR-195, and miR-497 by silencing cell-cycle genes *Dlk1*, *Ccnd*, and *Cdc25* in quiescent SCs.[7,8] There are also reports that miR-431 mediates SC heterogeneity during muscle development and regeneration by targeting *Pax7*.[25] Other miRNAs, like miR-31, have been previously implicated in regulating the entry into the myogenic program during SC activation by targeting *Myf5* 3′UTR.[9] In this study, we found that miR-106b regulated both SC proliferation and myogenic progression *in vitro* and *in vivo*. As miR-106b was present only in MYF5^{neg} SCs and we have previously demonstrated that this miRNA targets cell-cycle regulatory genes,[11] we concluded that this miRNA played a specific role by

Figure 6. RNA-seq analysis of antimiR-106b and scramble administration effects during muscle regeneration in mdx mice after CTX injury

(A) Schematic representation of antimiR-106b/scramble administration and RNA-seq analysis (n = 3 per time point and condition). (B) Volcano plots showing differentially expressed genes in AntimiR-106b versus Scramble-treated dystrophic muscles at day 3 after CTX injection, AntimiR-106b versus Scramble-treated dystrophic muscles at day 7 after CTX injection, and differentially expressed genes in antimiR-106b-treated dystrophic muscles at day 3 versus day 7 after CTX injection and Scramble-106b-treated dystrophic muscle at day 3 versus day 7 after CTX injury. (C) GO-biological process and cellular component ORA-analysis in antimiR-106b treated muscles between day 3 and day 7 after CTX injury. (D) GO-biological process and cellular component ORA-analysis in scramble-treated muscles between day 3 and day 7 after CTX injury. (E) GO-biological process and cellular component ORA-analysis shared by antimiR-106b and scramble-treated muscles between day 3 and day 7 after CTX injury.

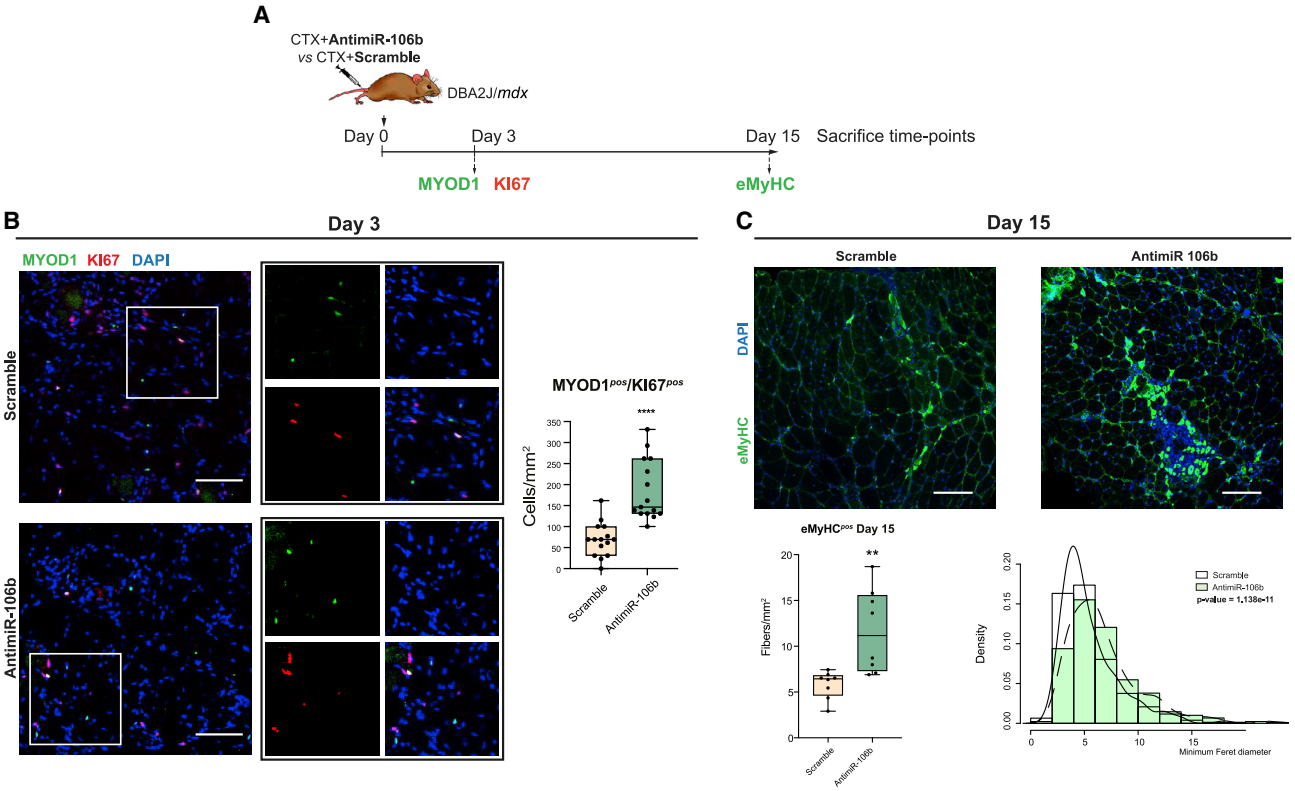

Figure 7. miR-106b inhibition *in vivo* increases muscle regeneration in the DBA/mdx mice

(A) Scheme of the CTX + antimiR injection in the DBA2J/mdx male mice TA. CTX was injected together with antimiR molecules in TA; scramble and CTX were injected into the contralateral muscle and used as a control. n = 8 DBA2J/mdx mice, aged 4–6 months, were randomized into two groups: CTX + scramble versus CTX + antimiR injected at 3 days post-injection and scramble versus CTX + antimiR injected at 15 days post-injury (n = 4 per time point in each group). (B) MYOD1 and KI67 immunostaining on the TA section from the scramble- and antimiR-treated DBA2J/mdx mice (3 days post-administration). Quantification of the number of $MYOD1^{pos}/KI67^{pos}$ cells is shown. (C) Immunostaining for $eMyHC^{pos}$ in the scramble and antimiR-treated DBA2J/mdx mice. Percentage of $eMyHC^{pos}$ myofibers and muscle fiber size distribution analyzed by Minimal Feret Diameter (μm) are shown. Scale bars, 120 μm (B), 40 μm (C). Data are presented as mean ± SD. **p < 0.01; ****p < 0.0001.

controlling quiescence versus cell activation in $MYF5^{neg}$ SCs. As we observed the good capability of miR-106b compared with the other miRNAs (miR-31) targeting *Myf5*, we propose that miR-106b could act by reinforcing MYF5 inhibition in a subset of a highly quiescent SC population. However, as miRNAs may have multiple potential targets, the possibility that other miR-106b targets may contribute to the observed effects could not be excluded. In addition, because fluorescence *in situ* hybridization (FISH) amplification system used for miRNA detection in this study did not enable us to clearly discern miR-106b staining in cytoplasm and/or nucleus of SCs; we cannot rule out that the effects mediated by miR-106b in these cells can be induced both in nucleus and cytoplasm, as previously reported for other cell types.[26]

Research conducted to understand the mechanisms controlling SC behavior in response to muscle injury has drawn considerable interest because emerging studies have pointed out that an altered SC function is associated with skeletal muscle atrophy in chronic illness, disuse, aging, and other muscle degenerative diseases.[27–29] Therefore, the enhancement of intrinsic factors within SCs may address impaired cell proliferative capacity and differentiation, and might improve skeletal muscles' regenerative response. We provide evidence that miR-106b inhibition by an antimiR intramuscular injection enhanced the regenerative potential of mouse MuSCs by amplifying the proliferative myogenic-committed population in early muscle regeneration phases. Interestingly with a single antimiR injection, muscle regeneration enhancement became even more pronounced after a second round of injury. In the adult muscle, muscle $PAX7^{pos}$ SCs coexisted with a small subpopulation of committed $MYOD1^{pos}$ SCs ready for immediate differentiation without preceding cell division.[16] We found that the number of $PAX7^{pos}$ sublaminar cells increased after 30 days of muscle injury in antimiR-treated muscles, with no changes in $MYOD1^{pos}$ sublaminar cells, plus a tendency to generate a large amount of $PAX7^{pos}$ cells that was conserved after re-injury was also observed. Those results, together with the fact that miR-106b inhibition facilitates asymmetric division in cultured SCs, led us to think that antimiR treatment could contribute mainly to extend stem SC populations, which display good engraftment capability, but also contribute to differentiated myofibers.[6] We also show for the first time the

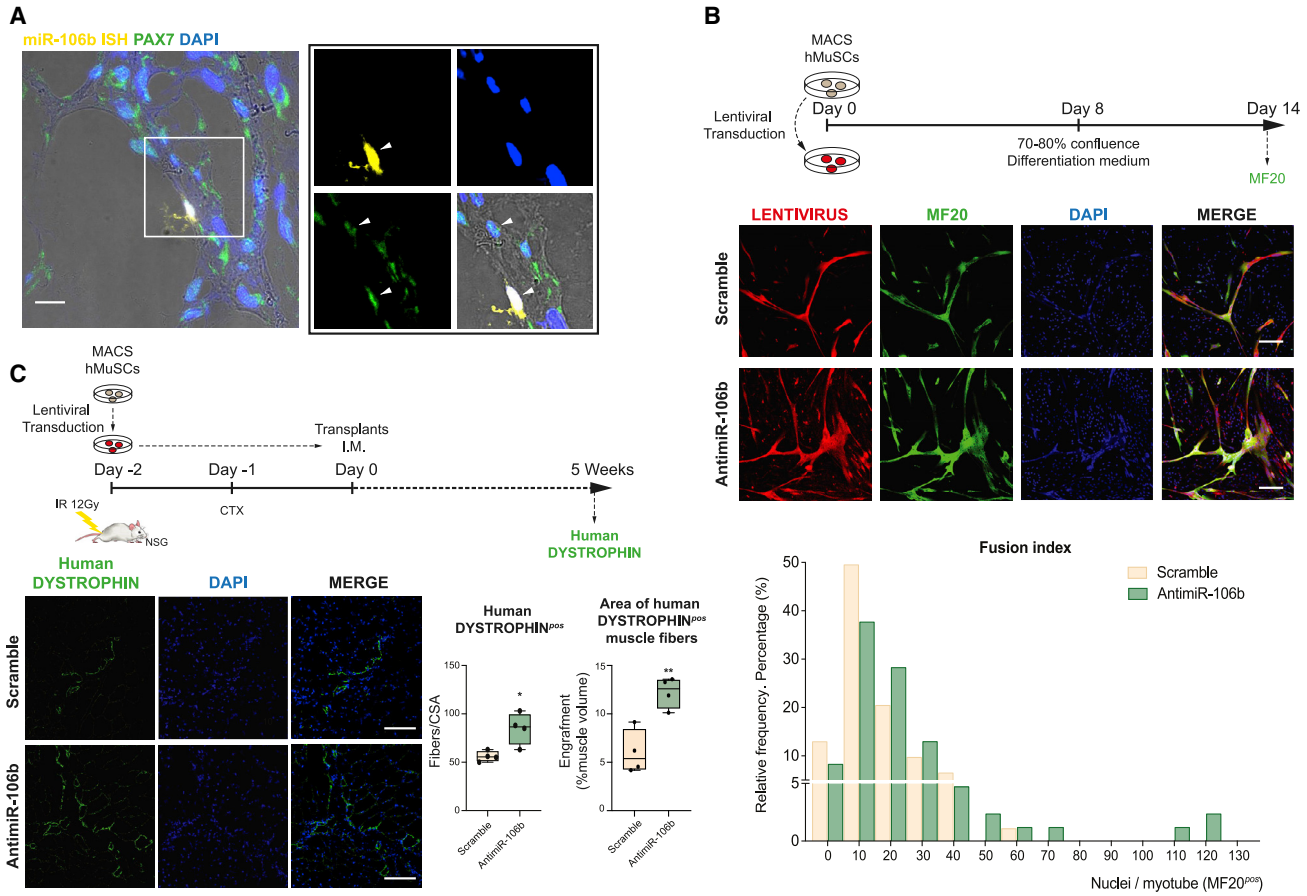

Figure 8. miR106b is expressed in hMuSC and its inhibition enhances hMuSC myogenic differentiation potential and promotes their engraftment after cell transplantation *in vivo*

(A) Fluorescence *in situ* hybridization for the miR-106b and immunofluorescence staining of PAX7 on the human muscle section. (B) Scheme of the antimiR-106b hMuSCs-treated cells (30,000–40,000 cells) and MF20 staining; the quantification of the fusion index is shown (n = 3 experimental replicates; 15 fields per plate). (C) Scheme of the antimiR-treated hMuSC transplantation in NSG mice; n = 4 NGS male mice (Scramble-transfected cells were transplanted into the contralateral muscle and used as a control), and immunostaining for human DYSTROPHIN in the TA section from the transplanted NGS mice. The quantification of the human-DYSTROPHIN^{pos} myofibers and the extend of myoblast engraftment (area of human dystrophin positive muscle fibers) are shown. Scale bars, 20 μm (A), 200 μm (B), and 120 μm (D). Data are presented as mean ± SD. *$p < 0.05$.

importance of miRNA inhibition for increasing the regenerative potential of hMuSCs, which indicates the relevance of miR-106b inhibition for the future development of novel therapeutic approach to improve muscle regeneration.

It is also apparent that myopathies like DMD significantly impair the regenerative process due to a low proliferative potential and poor progenitor formation from mdx-SCs.[4,12] The importance of miRNA ameliorating muscular dystrophy in mdx mice has been previously highlighted in the search for new therapeutic strategies to target SC defects in DMD. miR-206 delays muscular dystrophy progression in mdx mice by promoting SC differentiation by targeting *Notch3*, *Pax7,* and *IGFbp5*.[30] Transgenic mdx mice that overexpress miR-431 lessen dystrophic phenotype severity.[25] Our analysis revealed miR-106b to be inherently up-regulated in dystrophic murine SCs. As we previously documented that PITX2 represses miR-106b expression in SCs,[11] increased miR-106b levels could be due to the decreased *Pitx2* expression in mdx muscles, as our group also previously reported.[12] One remarkable finding in the present work was that miR-106b inhibition in mdx mice after muscle injury increased the number of myogenic progenitors, enhanced muscle regeneration, and promoted functional rescue. The transcriptomic analysis further emphasized the notion that miR-106b inhibition led to enrich the transcriptional program associated with skeletal muscle differentiation after injury in mdx mice. We also observed that biological process linked to impaired muscle regeneration in DMD, such as inflammatory response, are enriched in scramble-treated control but not in antimiR-treated mdx mice after muscle injury. Therefore, we believe that the increased muscle regeneration after antimiR treatment in mdx mice might be also minimizing degenerative

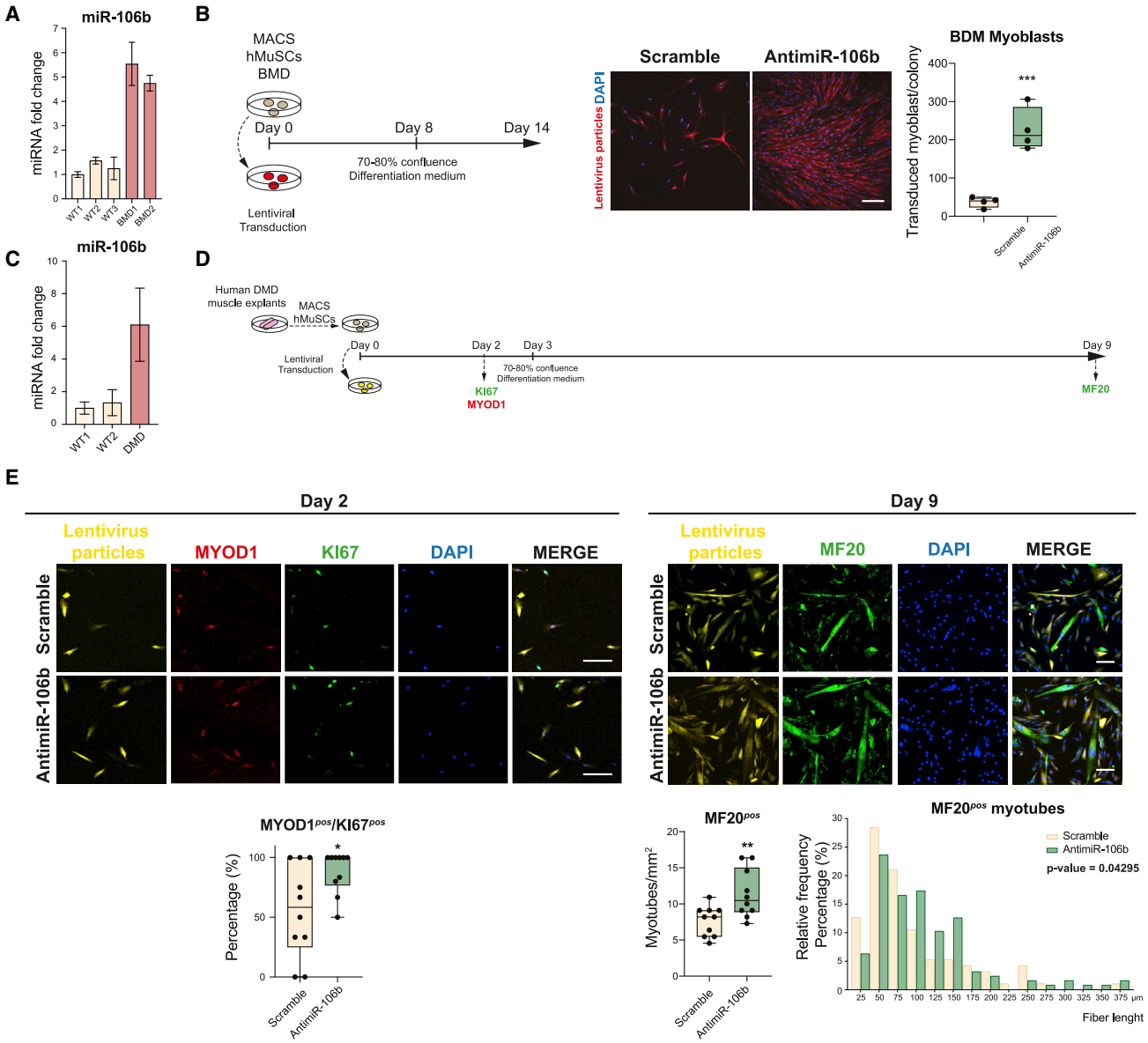

Figure 9. antimiR-106b treatment increases the myogenic differentiation of BMD hMuSCs and increases the capabilities to proliferate and to form the myogenic precursors of DMD hMuSCs

(A) Transcript levels of miR-106b in muscle biopsies from control patients (n = 3 male, 31, 35, and 40 years old [CT1, CT2, and CT3, respectively]) and two BMD patients (male, 32 and 35 years old [BMD1 and BMD2, respectively]). Error bars in RT-qPCR analysis show the technical SD deviation of each patient. (B) Scheme of hMuSC isolation from BMD muscles biopsies, antimiR treatment by lentiviral transduction, and the quantification of the number of transducted-myoblasts per cell colony (day 14 after lentiviral transduction). (C) Transcript levels of miR-106b in fresh isolated $CD56^{pos}$ hMuSCs from control biopsies (n = 2 male, 35 and 40 years old [CT4 and CT5, respectively]) and from DMD biopsy (male, 5 years old). Error bars in RT-qPCR analysis show the technical SD deviation of each patient. (D) Scheme of hMuSCs isolation from the DMD muscle biopsies and antimiR or Scramble treatment by lentiviral transduction. (E) Immunostaining for MYOD1 and KI67 on day 2 after lentiviral transduction. MF20 staining of the myotubes derived from the transducted dystrophic hMuSCs at 9 days post-transduction. The percentage of the $KI67^{pos}/MYOD1^{pos}$ cells on day 2 and the number of $MF20^{pos}$ myoblasts as well as fiber length distribution on day 9 are shown. 30,000–40,000 cells; n = 3 experimental replicates; 10 fields per plate. Scale bars, 50 μm. Data are presented as mean ± SD. *p < 0.05; **p < 0.01; ***p < 0.001.

transcriptional pathway response previously identified in the muscles of dystrophic mice, such as the inflammatory response.[31] More importantly, we demonstrated that miR-106b inhibition in hMuSCs isolated from patients with BMD and DMD improved the inherent defects linked to their proliferation capability and proper differentiation.

In conclusion, we demonstrate that miR-106b is an important modulator of SC behavior, acting as a quiescence regulator in a subset of the SC population, and its inhibition is required for proper muscle regeneration. The main finding, based on miRNA modulation in mouse and human dystrophic SCs, identifies miR-106b as a new candidate to develop novel therapeutic strategies that increase the regeneration capacity of the damaged muscle in DMD. Although the newly generated muscle will still show lack of dystrophin, increased skeletal muscle regeneration after antimiR treatment may compensate muscle fiber loss, ameliorating thus regenerative stimulus and minimizing the risk of SC depletion in DMD. Furthermore, the possibility of SC exhaustion after short-term antimir treatment is reduced since we observed that the amount of $Pax7^{pos}$ cells in the muscle stem cell niche was enlarged in antimiR-injected muscles after re-injury. Therefore, antimiR-106b treatment could, at least temporarily, increase muscle mass, making it better able to respond to gene therapy.

MATERIAL AND METHODS

All the employed reagents and materials are listed in Tables S1 and S2.

Cell lines, animals, and human samples

Cell lines Sol8 and HEK293T were purchased from ATCC and kept in culture in line with the manufacturer's instructions. The animal procedures were approved by the University of Jaen Ethics Committee, and were conducted according to national and European community guideline regulations for animal care and handling inside an animal facility at the Universities of Jaen (UJA) and Granada (UGR). C57BL/6J and C57BL/10ScSn-Dmd^{mdx}/J (henceforth mdx) mice were supplied by the Jackson Laboratory. DBA2J/mdx mice were kindly provided by the laboratory of Pura Muñoz-Canoves. NOD.Cg-$Prkdc^{scid}Il2rg^{tm1Wjl}$/SzJ (henceforth NSG) mice were provided by the UGR. The use of human sample collection was approved by the Human Research Ethics Committee of UGR. Biopsies were obtained from informed patients or their legal guardian's consent. Detailed information is listed in Table S1. The study was performed in accordance with the ethical standards laid down in the 1975 Declaration of Helsinki and approved by the Ethics Committee at the University of Jaen and Hospital Universitario Virgen de las Nieves from Granada. Informed consent was obtained from all participants.

Mouse and human SC isolation and culture

For mouse SC isolation, hindlimb muscles from 4- to 5-month-old male (C57BL/6 and mdx) mice were collected. Muscles were transferred and minced on a dish with DMEM:F12 (1:1). Minced muscles were dissociated 1 h at 37°C in an enzymatic solution containing DMEM:F12 (1:1) supplemented with 1 mg/mL collagenase type D and 4% Trypsin solution. Afterward, mechanical dissociation was performed through 14-G and 18-G needle up and down. For each step of mechanical dissociation, muscle mixture was decanted 5 min and supernatant was collected to a new tube with 5 mL of fetal bovine serum (FBS). Supernatant-FBS suspension was filtered through 100-μm and 40-μm cell strainers. Suspension cells were centrifuged at 300 × *g* for 5 min and then the pellet was resuspended with 1 mL of PBS. Red Blood Cells Lysis Solution (130-094-183; Miltenyi Biotec) was incubated for 2 min. Incubation with magnetic labeling was performed for 15 min at 4°C of 1:5 dilution according MicroBeads Satellite Cell Isolation Kit (negative selection with Satellite Cell Isolation Kit-130-104-268, and positive selection with Anti-Integrin α-7 MicroBeads-130-104-261; Miltenyi Biotec). LS and MS Columns were pre-equilibrated and placed in appropriate magnets, and cell suspension was applied onto the column. Purified mouse SCs (5,000–10,000 cells) were seeded on 0.1% gelatin coated μ-Dish 50 mm (Ibidi, 81136) and cultured in mouse growth medium (mouse-GM) containing DMEM GlutaMAXTM (Life Technologies) and DMEM:F12 (Lonza) 50:50 supplemented with 20% FBS (Sigma), 2% Ultroser G (Pall), 3% penicillin/streptomycin (P/S), and incubated at 37°C, 5% CO_2. For myoblast differentiation, when 70% to 80% confluence is reached, the medium was changed decreasing to 2% FBS.

For BMD, and control hMuSC experiments, isolation was done by MACS, as previously described for mice. In this case, negative cell sorting was performed using CD45 and CD31 human MicroBeads (130-045-801 and 130-091-935; Miltenyi) and positive cell sorting was performed using CD56-human MicroBeads (130-050-401; Miltenyi). DMD and their controls, hMuSCs were isolated from fresh muscle biopsies as follows. Muscle fascicles were released and cuted into 3-mm fragments in HBSS supplemented with 1% PSF (P/S-Fungizone). Fascicles were incubated overnight at 37°C, 5% CO_2 in conditioning medium containing M199 (Gibco) supplemented with 37.5% FBS and 1% PSF. Next day, explants were seeded on plates coated with 25% v/v fresh human plasma until cell growth appeared. Subsequently, explants were cuted into 1-mm-length fragments and cultured on 33.3% v/v fresh human plasma-1.5% gelatin type-A (Sigma) coated plates until the cell monolayer appeared around explants. Positive cell sorting was performed using CD56-human MicroBeads (130-050-401; Miltenyi). $CD56^{pos}$ hMuSCs cells were seeded on 0.1% gelatin type-A coated plates and cultured in human growth medium (human-GM) containing 75% DMEM and 25% M199 supplemented with 10% FBS, 50 μg/mL insulin, 0.25 μg/mL human-FGF2, 0.02 μg/mL human-EGF, 2 mM L-glutamine, and 1% PSF. Cells were incubated at 37°C, 5% CO_2 until 50% to 60% of confluence was reached. For myoblast differentiation 70% to 80% confluence should be reached and human-GM was substituted with one supplemented with 2% FBS, 50 μg/mL insulin, 2 mM L-glutamine, and 1% PSF.

Single myofiber isolation and culture

Isolated single myofibers were obtained from extensor digitorum longus (EDL) of 4-month-old C57BL/6 mice as previously described in the protocol by Zammit's lab with slight variations.[32] After dissection, EDL was incubated in 0.2% w/v collagenase type I (17100017, Gibco)/DMEM for 1 h 30 min in a 37°C water bath. Digestion was stopped when the muscle started to loosen up. EDLs were transferred to a pre-warmed dish with DMEM supplemented with 1% P/S. After 30 min of muscle rest, mechanical dissociation was performed to release individual myofibers, flushing with a bore glass pipette (the dishes were returned to the incubator every 10 min for 10 min to keep them warm). Single myofibers were transferred through three new pre-warmed dishes for clean-up. Immediately, single myofibers were fixed

for analysis at 0 h or cultured for 48 h in high serum medium (DMEM-high glucose, GlutaMAX supplemented with 10% horse serum, 0.5% chicken embryo, and 1% P/S). Horse serum was used on plates and glass pipettes as coating substrate for floating condition and to avoid stuck fibers.

Lentiviral transduction

Lentivirus particles expressing eGFP or mCherry Fluorescent Protein were produced using Lenti-Pac HIV Expression Packaging Kit (LT001, GeneCopoeia). Briefly, HEK293T cells (ATCC) were transfected with three plasmids encoding the vector components: mimic hsa-mir-106b (HmiR0111-MR11 from GeneCopoeia, onwards pre-miR-106b), inhibitor of hsa-miR-106b (HmiR-AN0029-AM03 from GeneCopoeia, onwards antimiR-106b) or control microRNA (CmiR-AN0001-AM03 from GeneCopoeia, onwards Scramble), plasmid CMV-eGFP was used as a transfection control. Infectious lentivirus were harvested at 48 h post-transfection, filtered through 0.22 μm and stored at −80°C. Lentivirus was titrated by using the Lenti-PACTM HIV qRT-PCR Titration Kit (217LT005, GeneCopoeia). To infect cells, lentivirus was added at 200 MOI and transduction was monitored by fluorescence microscopy.

Lipofectamine transfections

Sol8 cell line were transfected with mirVana miRNAs: premiR-31 (4464066; Thermo), premiR-106b (4464067; Thermo), premiR-31 + premiR-106b and Scramble (4464077; Thermo) at 80 nM using Lipofectamine-2000 (Invitrogen) following the manufacturer's instructions. After 24 h, cells were collected for RNA extraction and RT-qPCR analysis.

Cell-cycle arrest

Fresh SCs from 1-month-old male C57BL/6 mice were isolated as previously described in this article. SCs were seeded in two μ-Dish 50 mm for lentivirus transfection with scramble or antimiR-106b diluted in mouse-GM. After 3 days of culture, SCs were attached, medium was refreshed, and cycle arrest was started as previously described.[15] Briefly, to inhibit DNA synthesis, SCs were treated with 2.5 mM thymidine for 16 h and released for 8 h, treated again with 2.5 mM thymidine for 16 h and released for 4 h. Afterward, to arrest cells during mitosis, SCs were treated with 68 μM monastrol for 8 h, released, and treated for 2 h with 10 μM MG132 to block the proteolytic activity of the 26S proteasome complex. Finally, cells were released for 1 h to synchronize activated SCs at the late telophase stage, cells were then fixed in 4% paraformaldehyde (PFA) for 10 min and immunocytochemistry was performed.

Gain- and loss-of-function *in vivo* analysis

For gain- and loss-of-function analysis, mice were anesthetized by using isoflurane, 2% to 5% inhaled, to a surgical plane of anaesthesia. Twenty-four C57BL/6, 15 mdx, and eight DBA2J/mdx mice were injected in each in each TA muscle with 50 μL of cardiotoxin solution (CTX; 10 μM) together with 11.55 μg of mirVana miRNAs (Thermo). This dose is equivalent to 0.57 mg per kg body weight.[33] Negative Control #1 Inhibitor (4464077) was used as Scramble, hsa-miR-106b-5p mimic (4464067) was used as premiR-106b and hsa-miR-106b-5p inhibitor (4464085) was used as antimiR-106b. Finally, an exhaustion treadmill trial was performed to evaluate the endurance of treated 4-month-old male mdx mice (and C57BL/6 mice were used as controls) fusing a motorized treadmill (Panlab Treadmills) supplied with a shocker plate as described previously.[34] The treadmill was run at 0° of inclination at 5 m/min for 5 min; subsequently, the speed was increased 1 m/min every minute. The test ended when the mouse remained more than 20 s on the shocker plate.

HMuSC xenotransplants

Xenotransplants were performed on 3-month-old NSG mice by intramuscular injection of antimiR-106b-tranducted hMuSCs. Briefly, 2 days before transplantation, TA irradiation (12 Gy) was done to incapacitate endogenous SCs, and hMuSCs were transfected with scramble or antimiR lentiviral particles *in vitro*. One day before transplantation, injury with CTX was done on each TA to induce regeneration. During transplantation day, 1,000 to 3,000 treated hMuSCs were collected on 50 μL of DMEM (Lonza) and injected using a 25-G needle into regenerating TA. Mice were killed 5 weeks after cell injection and TAs were harvested for histological analysis.

Muscle collection and processing

For tissue collection, mice were killed by cervical dislocation. TA from mice were collected and frozen in liquid nitrogen-cooled isopentane for sectioning or in liquid nitrogen for total RNA isolation. For histological analysis, tissue specimens were sliced using a cryostat microtome (CM1510S, Leica) to 8 μm thick and mounted onto Thermo Scientific SuperFrost Ultra Plus Adhesion Slides.

Fluorescence *in situ* hybridization

FISH for miRNA detection was performed in cryosections of TA muscle from C57BL/6 and mdx mice, and also on human sartorius muscle and isolated myofibers from C57BL/6. All the samples were post-fixed in 4% PFA, followed by washes in DEPC-treated PBS. To block endogenous peroxidase activity, a 10-min wash was done with 0.03% H_2O_2/PBS. Subsequently, permeabilization was performed with 2% acetone/PBS for 5 min. After one wash with 30% formamide/2× saline sodium citrate (SSC) buffer (300 mM NaCl, 30 mM Na_3 Citrate-2H_2O, pH 5) for 10 min, pre-hybridization was done for 30 min at 61°C with the hybridization mix (50% formamide, 1.3× SSC, 0.5 mg/mL yeast tRNA, 0.2× CHAPS, 0.5M EDTA NaOH, pH 8, and 0.2% v/v Tween-20). Hybridization was performed with 25 nM of the hsa-miR-106b-5p double DIG-labeled LNA probe (339111 YD00618264-BCG; Qiagen) diluted in hybridization mix at 61°C for 2 h and 30 min. Samples were then washed in 2× SSC and 1× SSC, at 61°C and the last wash at room temperature (RT). Samples were rinsed with 1× PBS prior to Alexa Fluor Tyramide SuperBoost Kit protocol (B40943 or B40912; Invitrogen). Briefly, samples were blocked for 1 h with Blocking Buffer (Invitrogen) and rinsed three times with 1× PBS. The corresponding anti-Digoxigenin antibody (rabbit-9H27L19 or mouse-ab420) was incubated at 5 μg/mL diluted in Blocking Buffer overnight at 4°C. The next day, samples were rinsed three times with 1× PBS and then were

incubated with the corresponding poly-HRP-conjugated secondary antibody (rabbit-B40943 or mouse-B40912) at RT for 60 min. Samples were rinsed three times with 1× PBS and the Tyramide Working Solution was added 8 min at RT following the manufacturer's instructions. Stop Reagent was added on top for 30 s and samples were rinsed in 1× PBS prior to immunostaining.

Hematoxylin-eosin staining and immunostaining

For H&E staining, the cryosection samples were pre-fixed with 4% PFA for 10 min at RT. After several washes in water, samples were incubated for 10 min with Mayer's Hematoxylin Solution until nuclei were stained. Activated Eosin Y Solution 0.5% was incubated for 10 min. Then several washes with water were performed prior to dehydration and DPX was used as mounting media. Images were captured with a 2.0-MP digital microscope camera, which was attached via a c-mount to the side port of a Motic AE2000 microscope.

For immunocytochemistry purposes, cultured cells and isolated myofibers were fixed with 4% PFA for 10 min and were then permeabilized with PBS, 0.25% Triton X-100, and 50 mM NH_4Cl for 10 min at RT. Samples were blocked with Blocking Solution containing 0.2% gelatin/PBS (G1393) for 20 min at RT. Primary antibodies (listed in Table S2) were added at 5 to 10 μg/mL in Blocking Solution overnight at 4°C. Alexa-conjugated secondary antibodies diluted 1/300 in Blocking Solution were added for 30 min at RT. For immunohistochemistry, the cryosection samples were fixed in 4% PFA for 10 min at RT. For the PAX7, PS6, and MYOD1 immunostaining, epitopes were unmasked in citrate buffer (10 mM sodium citrate, 0.05% Tween-20, pH 6.0) in a pre-heated water bath for 30 min at 96°C. Afterward, all the samples were pre-incubated in TBSA-BSAT (10 mM Tris, 0.9% NaCl, 0.02% sodium azide, 2% BSA, and 0.1% Triton-X100) for 30 min at RT. Primary antibodies (listed in Table S2) were diluted to 5 to 10 μg/mL in TBSA-BSAT and incubated overnight at 4°C in a humidified chamber. The next day, Alexa-Fluor-conjugated secondary antibodies diluted 1/200 in TBSA-BSAT were incubated for 2 h at RT. Finally, for both immunostaining protocols, samples were incubated in a 1/2,000 DAPI/PBS dilution for 15 min at RT. Hydromount was used for mounting and images were acquired by a Leica TCS SPE-CTR6500 Confocal Microscope.

Human myoblast in-cell western assay: myoblot

For the in-cell western assay, human DMD patient myoblasts (exon 48–50 deletion) were requested from the Queen Square Centre for Neuromuscular Disorders BioBank (CNMD Biobank, London, UK). Myoblasts were maintained in Skeletal Muscle Cell Growth Medium (PromoCell) supplemented with 10% FBS, GlutaMAX, 1× MEM NEAA, 1% P/S, and incubated at 37°C in 5% CO_2.

Human myoblasts were seeded at 7,500 cells/well on a 96-well plate previously coated with Matrigel in Skeletal Muscle Cell Growth Medium. After 24 h, when confluence was reached, medium was replaced with differentiation medium (DMEM-Lonza, 20% horse serum, and 1% P/S). After 24 h, cells were transfected with premiR-106b, antimiR-106b and Scramble at 40 nM using Lipofectamine 2000. Briefly, the medium was replaced with fresh differentiation medium at 5 h post-transfection. After a 7-day incubation period to allow myotube formation, cells were fixed by adding ice-cold methanol for 10 min at RT and were then washed with 1× PBS. For the in-cell western assay, cells were permeabilized with 1× PBS-Tween 0.1% Triton and then incubated with Odyssey Blocking Buffer (LI-COR Biosciences) for 2 h. After blocking, MF20 (DSHB) primary antibody diluted 1:100 in Odyssey Blocking Buffer was added for an overnight incubation at 4°C. The next day, plates were washed with PBS-Tween 0.1% and then treated with the secondary antibody mix IRDye 800CW goat anti-mouse and CellTag 700 Stain (LI-COR Biosciences) for 1 h at RT. Then, incubation plates were washed again with PBS-Tween 0.1% solution and were scanned by Odyssey CLx Imager (LI-COR Biosciences).

mRNA and miRNA extraction and RT-qPCR

Muscle total RNA was extracted from the treated TA muscles by the Direct-zol RNA MiniPrep-Zymo Research Kit (R2050; Zymo Research) following the manufacturer's instructions. Cells' total RNA was extracted from SCs by the RNAqueous-Micro Kit (AM1931; Thermo-Fisher Scientific) following the manufacturer's instructions. Either 500 ng of the total RNA from muscles or 50 ng of the total RNA from SCs were used as an mRNA retrotranscription template with the Maxima First Strand cDNA Synthesis Kit for RT-qPCR (K1642; Thermo-Fisher Scientific) in line with the manufacturer's instructions. For miR retrotranscription, 10 ng of total mRNA from muscles or SCs were used as the miR retrotranscription template with the miRCURY LNA Universal RT Kit (203301; Qiagen).

The qPCRs for the mRNA measurements were performed by SsoFast EvaGreen Supermix (1725201; Bio-Rad). The qPCR program consisted of 95°C for 30 s (initial denaturalization), followed by 40 cycles of 95°C for 5 s (denaturalization); 60°C for 10 s (annealing); 75°C for 7 s (extension). Finally, melt curves were determined by an initial step of 95°C for 5 s, followed by 0.5°C increments for 7 s from 65°C to 95°C. The relative level of each gene expression was calculated as the ratio of the extrapolated levels of each gene expression, with the Gapdh and Gusb genes as normalizers (both transcripts present constant expression stability, indicating their suitability as reference genes, Figure S2G). Primers used for the mRNA qPCR are listed in Table S3.

The qPCRs for the miRs measurements were performed by GoTaq qPCR Master Mix (A6001, Promega). The qPCR program consisted of 95°C for 10 min (initial denaturalization), followed by 40 cycles of 95°C for 5 s (denaturalization); 60°C for 1 min (annealing and extension). Finally, melt curves were determined by an initial step of 95°C for 5 s, followed by 0.5°C increments for 7 s from 65°C to 95°C. The relative level of each miR gene expression was calculated as the ratio of the extrapolated levels of each gene expression and U6 as the normalizer. Primers were used for the microRNA qPCR are listed in Table S4.

All the qPCR reactions were performed in a Bio-Rad CFX384 Real-Time PCR system. Each PCR reaction was performed in triplicate and repeated in at least three different biological samples to obtain a representative average. Relative measurements were calculated as described by Pfaffl MW.[35]

RNA-seq analysis

For RNA-seq analysis, TA muscles from treated mdx mice (CTX + scramble versus CTX + antimiR-106b) were collected and total RNA was isolated using the Direct-zol RNA MiniPrep-Zymo Research Kit (three biological replicates). RNA samples were sent to the Centro de Análisis Genómico (CNAG, Barcelona Spain) for RNA sequencing. Subsequently, 200 ng of the total RNA were used to prepare the RNA-seq library with the TruSeq RNA sample prep kit (Illumina) according to the manufacturer's instructions. Paired-end (2×75) RNA sequencing was carried out by HiSeq 2000 (Illumina). For trimming and aligning raw data, fastq sequence reads were uploaded to the European version of the Galaxy platform (https://usegalaxy.eu/).[36] Reads were trimmed with the Trim Galore software (http://www.bioinformatics.babraham.ac.uk/projects/trim_galore/) and aligned to the built-in mouse reference genome mm10 with the RNA STAR Gapped-read mapper for the RNA-seq data (Galaxy Version 2.6.0b-2).[37] For the gene expression analysis, bam files were downloaded from the Galaxy server and further analyzed with the different RStudio packages downloaded from the Bioconductor website (http://bioconductor.org). Reads were assigned to genes by means of the "featureCounts" function of the "Rsubread" package, version 1.28.1,[38] and mouse annotation file release M19, GRCm38.p6 (ftp://ftp.ebi.ac.uk/pub/databases/gencode/Gencode_mouse/release_M19/). Only the mapped reads were used to calculate gene expressions. The library size of each experimental point ranged from 34816337 to 54599372 sequences.

The differential gene expression analysis was performed by the limma + voom linear modeling approach using the "edgeR" version 3.20.9 package, the "limma" version 3.34.9 package, and an empirical Bayes method for differential expression.[39-41] All the gene comparisons with a p value <0.05 and a fold change >2 were considered differentially expressed under the experimental conditions.

A functional enrichment analysis was performed by the Over Representation Analysis (ORA) Method using either the "enricher" function for the "H: hallmark gene set" of MSigDB or the "enrichGO" function "GO Biological Process gene set." Both functions appear in the "clusterProfiler" package version 3.6.0.[42,43] The gene sets with a p value <0.05 were considered overrepresented under the experimental conditions.

Quantification and statistical analysis

Two-tailed unpaired Student's t test or Kolmogorov-Smirnov test were performed to calculate p values and to determine statistically significant differences. The number of independent experimental replications, mean ± SD, and statistical tests (p value) are reported in figure legends. Statistical analyses were performed with GraphPad Prism and RStudio. Images were processed for quantification by ImageJ software.

Data and software availability

The RNA-seq data reported in this paper are available under GEO accession number GSE134111.

SUPPLEMENTAL INFORMATION

Supplemental information can be found online at https://doi.org/10.1016/j.omtn.2022.08.025.

ACKNOWLEDGMENTS

We acknowledge Pura Muñoz-Canoves (University of Pompeu Fabra, Barcelona) for kindly providing us with DBA2J/mdx mice, and Carmen Paradas (IBiS-Sevilla) for the DMD muscle explants.
This work was partially supported by grants, BFU2015-67131 (Spanish Ministry of Economy and Competitiveness), PID2019-107492GB-100 (Spanish Ministry of Science and Innovation), Duchenne Parent Project Spain-2016 and 2019 grants, Carlos III Health Institute (ISCIII, Spain) and European Regional Development Funds (ERDF/FEDER) (Grants CP12/03057, CPII17/00004), and Ikerbasque (Basque Foundation for Science). L.R.O. holds an FPU17/03843 and P.S.M a CM19/00104 Fellowship.

AUTHOR CONTRIBUTIONS

Conceptualization, A.E.A.; Methodology, L.R.O., F.H., A.R., P.S., and V.A. Writing – Original Draft, A.E.A., F.H., and L.R.O.; Writing – Review & Editing, D.F. and A.E.A.; Validation: L.R.O., F.H., A.R., and V.A.; Formal Analysis: L.R.O., F.H., A.R., F.R., and V.A.; Investigation: L.R.O., F.H., F.R.A., P.S., V.A., C.C., A.C., and A.E.A.; Resources: C.C, A.C., M.M., and L.S. Visualization: L.R.O, F.H., D.V., P.S., and V.A; Supervision: D.F. and A.E.A.; Project Administration: A.E.A.; Funding Acquisition, D.F. and A.E.A.

DECLARATION OF INTERESTS

The authors declare no competing interests.

REFERENCES

1. Emery, A.E. (1991). Population frequencies of inherited neuromuscular diseases–a world survey. Neuromuscul. Disord. *1*, 19–29.
2. Blat, Y., and Blat, S. (2015). Drug discovery of therapies for Duchenne muscular dystrophy. J. Biomol. Screen *20*, 1189–1203.
3. Chang, N.C., Chevalier, F.P., and Rudnicki, M.A. (2016). Satellite cells in muscular dystrophy - lost in polarity. Trends Mol. Med. *22*, 479–496.
4. Dumont, N.A., Wang, Y.X., von Maltzahn, J., Pasut, A., Bentzinger, C.F., Brun, C.E., and Rudnicki, M.A. (2015). Dystrophin expression in muscle stem cells regulates their polarity and asymmetric division. Nat. Med. *21*, 1455–1463.
5. Feige, P., Brun, C.E., Ritso, M., and Rudnicki, M.A. (2018). Orienting muscle stem cells for regeneration in homeostasis, aging, and disease. Cell Stem Cell *23*, 653–664.
6. Kuang, S., Kuroda, K., Le Grand, F., and Rudnicki, M.A. (2007). Asymmetric self-renewal and commitment of satellite stem cells in muscle. Cell *129*, 999–1010.
7. Cheung, T.H., Quach, N.L., Charville, G.W., Liu, L., Park, L., Edalati, A., Yoo, B., Hoang, P., and Rando, T.A. (2012). Maintenance of muscle stem-cell quiescence by microRNA-489. Nature *482*, 524–528.
8. Sato, T., Yamamoto, T., and Sehara-Fujisawa, A. (2014). miR-195/497 induce postnatal quiescence of skeletal muscle stem cells. Nat. Commun. *5*, 4597.
9. Crist, C.G., Montarras, D., and Buckingham, M. (2012). Muscle satellite cells are primed for myogenesis but maintain quiescence with sequestration of Myf5 mRNA targeted by microRNA-31 in mRNP granules. Cell Stem Cell *11*, 118–126.

10. Baghdadi, M.B., and Tajbakhsh, S. (2018). Regulation and phylogeny of skeletal muscle regeneration. Dev. Biol. *433*, 200–209.

11. Lozano-Velasco, E., Vallejo, D., Esteban, F.J., Doherty, C., Hernández-Torres, F., Franco, D., and Aránega, A.E. (2015). A Pitx2-MicroRNA pathway modulates cell proliferation in myoblasts and skeletal-muscle satellite cells and promotes their commitment to a myogenic cell fate. Mol. Cell Biol. *35*, 2892–2909.

12. Vallejo, D., Hernández-Torres, F., Lozano-Velasco, E., Rodriguez-Outeiriño, L., Carvajal, A., Creus, C., Franco, D., and Aránega, A.E. (2018). PITX2 enhances the regenerative potential of dystrophic skeletal muscle stem cells. Stem Cell Rep. *10*, 1398–1411.

13. Beauchamp, J.R., Heslop, L., Yu, D.S., Tajbakhsh, S., Kelly, R.G., Wernig, A., Buckingham, M.E., Partridge, T.A., and Zammit, P.S. (2000). Expression of Cd34 and Myf5 defines the majority of quiescent adult skeletal muscle satellite cells. J. Cell Biol. *151*, 1221–1234.

14. García-Prat, L., Perdiguero, E., Alonso-Martín, S., Dell'Orso, S., Ravichandran, S., Brooks, S.R., Juan, A.H., Campanario, S., Jiang, K., Hong, X., et al. (2020). FoxO maintains a genuine muscle stem-cell quiescent state until geriatric age. Nat. Cell Biol. *22*, 1307–1318.

15. Liu, W., Wen, Y., Bi, P., Lai, X., Liu, X.S., Liu, X., and Kuang, S. (2012). Hypoxia promotes satellite cell self-renewal and enhances the efficiency of myoblast transplantation. Development *139*, 2857–2865.

16. Yin, H., Price, F., and Rudnicki, M.A. (2013). Satellite cells and the muscle stem cell niche. Physiol. Rev. *93*, 23–67.

17. Dumont, N.A., and Rudnicki, M.A. (2016). Targeting muscle stem cell intrinsic defects to treat Duchenne muscular dystrophy. NPJ Regen. Med. *1*, 16006.

18. Blau, H.M., Webster, C., and Pavlath, G.K. (1983). Defective myoblasts identified in Duchenne muscular dystrophy. Proc. Natl. Acad. Sci. USA *80*, 4856–4860.

19. Rodgers, J.T., King, K.Y., Brett, J.O., Cromie, M.J., Charville, G.W., Maguire, K.K., Brunson, C., Mastey, N., Liu, L., Tsai, C.-R., et al. (2014). mTORC1 controls the adaptive transition of quiescent stem cells from G0 to G(Alert). Nature *510*, 393–396.

20. Abdel-Salam, E., Abdel-Meguid, I., and Korraa, S.S. (2009). Markers of degeneration and regeneration in Duchenne muscular dystrophy. Acta Myol. *28*, 94–100.

21. Coley, W.D., Bogdanik, L., Vila, M.C., Yu, Q., Van Der Meulen, J.H., Rayavarapu, S., Novak, J.S., Nearing, M., Quinn, J.L., Saunders, A., et al. (2016). Effect of genetic background on the dystrophic phenotype in mdx mice. Hum. Mol. Genet. *25*, 130–145.

22. Fukada, S.i., Morikawa, D., Yamamoto, Y., Yoshida, T., Sumie, N., Yamaguchi, M., Ito, T., Miyagoe-Suzuki, Y., Takeda, S., Tsujikawa, K., and Yamamoto, H. (2010). Genetic background affects properties of satellite cells and mdx phenotypes. Am. J. Pathol. *176*, 2414–2424.

23. van Putten, M., Putker, K., Overzier, M., Adamzek, W.A., Pasteuning-Vuhman, S., Plomp, J.J., and Aartsma-Rus, A. (2019). Natural disease history of the D2-mdx mouse model for Duchenne muscular dystrophy. FASEB J. Off. Publ. Fed. Am. Soc. Exp. Biol. *33*, 8110–8124.

24. Gayraud-Morel, B., Chrétien, F., Jory, A., Sambasivan, R., Negroni, E., Flamant, P., Soubigou, G., Coppée, J.Y., Di Santo, J., Cumano, A., et al. (2012). Myf5 haploinsufficiency reveals distinct cell fate potentials for adult skeletal muscle stem cells. J. Cell Sci. *125*, 1738–1749.

25. Wu, R., Li, H., Zhai, L., Zou, X., Meng, J., Zhong, R., Li, C., Wang, H., Zhang, Y., and Zhu, D. (2015). MicroRNA-431 accelerates muscle regeneration and ameliorates muscular dystrophy by targeting Pax7 in mice. Nat. Commun. *6*, 7713.

26. Liu, H., Lei, C., He, Q., Pan, Z., Xiao, D., and Tao, Y. (2018). Nuclear functions of mammalian MicroRNAs in gene regulation, immunity and cancer. Mol. Cancer *17*, 64.

27. Blau, H.M., Cosgrove, B.D., and Ho, A.T.V. (2015). The central role of muscle stem cells in regenerative failure with aging. Nat. Med. *21*, 854–862.

28. McKenna, C.F., and Fry, C.S. (2017). Altered satellite cell dynamics accompany skeletal muscle atrophy during chronic illness, disuse, and aging. Curr. Opin. Clin. Nutr. Metab. Care *20*, 447–452.

29. Sousa-Victor, P., García-Prat, L., Serrano, A.L., Perdiguero, E., and Muñoz-Cánoves, P. (2015). Muscle stem cell aging: regulation and rejuvenation. Trends Endocrinol. Metabol. *26*, 287–296.

30. Liu, N., Williams, A.H., Maxeiner, J.M., Bezprozvannaya, S., Shelton, J.M., Richardson, J.A., Bassel-Duby, R., and Olson, E.N. (2012). microRNA-206 promotes skeletal muscle regeneration and delays progression of Duchenne muscular dystrophy in mice. J. Clin. Invest. *122*, 2054–2065.

31. Chemello, F., Wang, Z., Li, H., McAnally, J.R., Liu, N., Bassel-Duby, R., and Olson, E.N. (2020). Degenerative and regenerative pathways underlying Duchenne muscular dystrophy revealed by single-nucleus RNA sequencing. Proc. Natl. Acad. Sci. USA *117*, 29691–29701.

32. Moyle, L.A., and Zammit, P.S. (2014). Isolation, culture and immunostaining of skeletal muscle fibres to study myogenic progression in satellite cells. Methods Mol. Biol. *1210*, 63–78.

33. Trang, P., Wiggins, J.F., Daige, C.L., Cho, C., Omotola, M., Brown, D., Weidhaas, J.B., Bader, A.G., and Slack, F.J. (2011). Systemic delivery of tumor suppressor microRNA mimics using a neutral lipid emulsion inhibits lung tumors in mice. Mol. Ther. *19*, 1116–1122.

34. Benchaouir, R., Meregalli, M., Farini, A., D'Antona, G., Belicchi, M., Goyenvalle, A., Battistelli, M., Bresolin, N., Bottinelli, R., Garcia, L., and Torrente, Y. (2007). Restoration of human dystrophin following transplantation of exon-skipping-engineered DMD patient stem cells into dystrophic mice. Cell Stem Cell *1*, 646–657.

35. Pfaffl, M.W. (2001). A new mathematical model for relative quantification in real-time RT-PCR. Nucleic Acids Res. *29*, e45.

36. Afgan, E., Baker, D., Batut, B., van den Beek, M., Bouvier, D., Cech, M., Chilton, J., Clements, D., Coraor, N., Grüning, B.A., et al. (2018). The Galaxy platform for accessible, reproducible and collaborative biomedical analyses: 2018 update. Nucleic Acids Res. *46*, W537–W544.

37. Dobin, A., Davis, C.A., Schlesinger, F., Drenkow, J., Zaleski, C., Jha, S., Batut, P., Chaisson, M., and Gingeras, T.R. (2013). STAR: ultrafast universal RNA-seq aligner. Bioinformatics *29*, 15–21.

38. Liao, Y., Smyth, G.K., and Shi, W. (2019). The R package Rsubread is easier, faster, cheaper and better for alignment and quantification of RNA sequencing reads. Nucleic Acids Res. *47*, e47.

39. Law, C.W., Chen, Y., Shi, W., and Smyth, G.K. (2014). voom: precision weights unlock linear model analysis tools for RNA-seq read counts. Genome Biol. *15*, R29.

40. Robinson, M.D., McCarthy, D.J., and Smyth, G.K. (2010). edgeR: a Bioconductor package for differential expression analysis of digital gene expression data. Bioinformatics *26*, 139–140.

41. Ritchie, M.E., Phipson, B., Wu, D., Hu, Y., Law, C.W., Shi, W., and Smyth, G.K. (2015). Limma powers differential expression analyses for RNA-sequencing and microarray studies. Nucleic Acids Res. *43*, e47.

42. Boyle, E.I., Weng, S., Gollub, J., Jin, H., Botstein, D., Cherry, J.M., and Sherlock, G. (2004). GO::TermFinder–open source software for accessing Gene Ontology information and finding significantly enriched Gene Ontology terms associated with a list of genes. Bioinformatics *20*, 3710–3715.

43. Yu, G., Wang, L.-G., Han, Y., and He, Q.-Y. (2012). clusterProfiler: an R package for comparing biological themes among gene clusters. OMICS A J. Integr. Biol. *16*, 284–287.